Quaternary International 581-582 (2021) 7–27

Contents lists available at ScienceDirect

Quaternary International

journal homepage: www.elsevier.com/locate/quaint

Human existence potential in Europe during the Last Glacial Maximum

Konstantin Klein [a,1], Christian Wegener [a,1], Isabell Schmidt [b,1], Masoud Rostami [a,1], Patrick Ludwig [c], Sven Ulbrich [a,d], Jürgen Richter [b,1], Gerd-Christian Weniger [e,1], Yaping Shao [a,*,1]

[a] Institute of Geophysics and Meteorology, University of Cologne, Cologne, Germany
[b] Department of Prehistoric Archaeology, University of Cologne, Cologne, Germany
[c] Institute of Meteorology and Climate Research, Karlsruhe Institue of Technology, Karlsruhe, Germany
[d] Deutscher Wetterdienst, Offenbach, Germany
[e] Neanderthal Museum, Mettmann, Germany

ARTICLE INFO

Keywords:
Human existence potential
Last glacial maximum (LGM)
Solutrean
Epigravettian
Environmental human catchment
Best potential path
Logistic regression

ABSTRACT

Archaeological records indicate that many regions in Europe remained unoccupied by hunter-gatherers during the Last Glacial Maximum (LGM), probably due to the harsh climatic conditions and glacial extent. In the populated regions of southwestern Europe, a new technocomplex, the Solutrean, is known to have emerged among hunter-gatherers but did not reach the regions east of 10°E. To better understand human occupation of Europe during the LGM, Human Existence Potential (HEP) is presented, which expresses the suitability of a region with given environmental conditions for habitation by hunter-gatherers. We estimate the HEP based on archaeological site locations and reconstructed climate/environment data. By geostatistically upscaling archaeological site distributions into Core Areas, we distinguish areas that were likely to have been continuously occupied by hunter-gatherers from areas intermittently occupied. The use of Core Areas in the model improves the description of regions of continuous human presence, removing some of the previously observed mismatches between reconstructions and archaeological records. Using HEP, important anthropological and archaeological questions can be studied. Environmental Human Catchment (EHC) and Best Potential Path (BPP) are applied to quantify an area of HEP attraction and the lowest-cost path between two areas, respectively. With these tools, we characterize the potential connections between the Core Areas, the environmental barriers and possible social and technological interactions. A clear difference in environmental adaptation is found between the populations in western and eastern Europe, with a significant climate barrier preventing the propagation of the Solutrean to eastern Europe.

1. Introduction

Human demography and adaptation during the Last Glacial Maximum (LGM) have been investigated intensively during the past decade using a diverse set of methods (Banks et al., 2009; Tallavaara et al., 2015; Maier et al., 2016; Burke et al., 2017; Bocquet-Appel et al., 2005; French and Collins, 2015; Weniger et al., 2019). Many researchers agree that hunter-gatherers in Europe were facing extreme climate during this time period with colder and drier conditions compared to the present-day (e.g., Bartlein et al., 2011; Annan and Hargreaves, 2013). Furthermore, evidence of human presence at the time is scarce for northern Europe, but more abundant for most parts of southwestern Europe, with the currently known distribution of archaeological sites probably shaped by the limits imposed by climatic conditions (see discussion in Tallavaara et al., 2015).

Cultural developments differed considerably within the inhabited regions. A suite of new lithic technologies and implements, the Solutrean technocomplex, appeared throughout southwestern Europe, with regionally distinct lithic point types presumably reflecting human adaptations to specific ecological niches (Banks et al., 2009; Schmidt, 2015b). In eastern Europe, the Epigravettian technocomplex constituted a cultural development strongly rooted in the preceding Gravettian. Studies about this large-scale division suggest an environmental rupture that separated the populations of the two regions (Banks et al., 2009;

* Corresponding author.
E-mail address: yshao@uni-koeln.de (Y. Shao).
[1] Member of the Collaborative Research Centre (CRC) 806, 'Our Way to Europe'.

https://doi.org/10.1016/j.quaint.2020.07.046
Received 14 October 2019; Received in revised form 15 July 2020; Accepted 25 July 2020
Available online 26 August 2020

Maier et al., 2016).

In contrast to scenarios of a population crisis during the LGM (Straus, 1990a, b; Tallavaara et al., 2015), diachronic studies on population size (e.g., Maier and Zimmermann, 2017; Maier et al., 2016; French and Collins, 2015) suggest that human populations had already experienced a massive decrease - local extinctions and a breakdown of trans-continental social networks - during the preceding final Gravettian period when the climate changed, insolation decreased, the vegetation-growth period shortened, and glaciers extended (Maier et al., 2020). Estimates indicate that populations recovered during the LGM, and the northern regions of Europe were finally repopulated during the succeeding Magdalenien. These Upper Paleolithic population changes in Europe have been illustrated by the repeated replacement model, as proposed by Bradtmöller et al. (2012).

To expand these insights and to further investigate human-environment interactions, we assume that (1) similar environmental conditions have the same potential for human existence and (2) they act as the dominant driver for human dispersal at the time. Working under these two premises, which are in line with many previous studies (van Andel and Davies, 2003; Bocquet-Appel et al., 2005; Tzedakis et al., 2007; Müller et al., 2011; Schmidt et al., 2012; Banks et al., 2013; Ludwig et al., 2018), we use a set of climate variablтes to estimate the Human Existence Potential (HEP), which defines the probability of hunter-gatherers existence for given technocomplexes, depending on available resources and climate and environment conditions. Resources in some areas are difficult to access, HEP is thus modified by additional parameters such as topography, glaciers, water bodies, and forests.

Using the HEP-model, we explore and quantify some important aspects of human-environment relations. Under the assumption that the mobility of hunter-gatherers - and thus contacts between groups - was facilitated by favorable environmental conditions at broader temporal and spatial scales, we consider a high HEP to positively affect the establishment and maintenance of human social networks. Kondo et al. (2018) suggested that paths along favorable environmental conditions can be used to describe migration routes between two points. This idea can be readily incorporated in HEP framework. The Best Potential Path (BPP) can be calculated by integrating HEP along the routes between two points. Note that this definition should be distinguished from the Least Cost Path - which is usually defined in archaeology by the walking speed in relation to the topography (e.g., White and Surface-Evans, 2012; Becker et al., 2017). We apply the BPP approach to the Solutrean network by calculating the BPP between the centres of different Core Areas. Furthermore, we analyze the cost of every BPP (T_{BPP}) to estimate the probability of contact between two Core Areas.

To gain further insight into population dynamics, we introduce a new concept, the Environmental Human Catchment (EHC), defined as an area delimited by minima in the HEP distribution. Our definition of catchments is different from that of Vita-Finzi et al. (1970), in which hunting-gathering and agricultural economies were considered. If the assumption that LGM hunter-gatherers preferred living in areas of high HEP is correct, their movements were probably oriented in the direction towards HEP maximums on longer time scales. Therefore, the HEP maximums define catchments and are used to identify the EHCs. The EHC corresponding to a HEP maximum is obtained by following the "upflow" of each grid point into the maximum. We assume that hunter-gatherers left an EHC only if forced to by external or internal factors such as environmental or socio-cultural factors.

To improve the previous approaches for characterizing environment conditions of LGM-human-occupation, we implement an up-scaling procedure of the archaeological data in the model. Given that the archaeological data, i.e., the geographic positions of sites dated to the LGM (Maier et al., 2016), constitute the evidence from a palimpsest of several thousand years, they probably contain outliers. The climate data used to derive the HEP, in contrast, represent large-scale and time-averaged conditions for the entire LGM. By spatially up- and temporally down-scaling archaeological data into Core Areas, the temporal scale coincides better with the temporal scale of the climate data. Such an up- and down-scaling procedure has been used in several studies (e.g., Zimmermann et al., 2004, 2009; Kretschmer, 2015). In a case-by-case analysis of the HEP, we compare the results obtained from all sites with those obtained from sites in Core Areas. By doing so, we identify the likely areas of continuous human settlement in Europe during the whole LGM period, and the likely areas of intermittent settlement during certain LGM phases when climate conditions were favorable.

2. Data

2.1. Archaeological data

The presence of hunter-gatherers was determined by using 396 archaeological sites across Europe assigned to the LGM (Maier and Zimmermann, 2015). This database is available online.[2] It specifies the geographical position and cultural attribution of each assemblage. It includes radiocarbon-dated sites from the period between 25 ka and 20 ka cal BP and sites typologically attributed to the Solutrean, Badegoulian or Epigravettian technocomplex. Due to constraints in the applied method and datasets in Italy and the Balkan region, these areas were excluded from the further analysis (cf. Discussion in Maier et al., 2016), reducing the archaeological sites from 396 to 358 in total (Fig. 1). We used two datasets to create and test the HEP model:

(i) Dataset All (DatALL): all sites of the dataset,
(ii) Dataset Core Areas (DatCA): sites located within Core Areas.

DatCA becomes a subset of DatALL by applying an up-scaling procedure to the archaeological data following the protocol described elsewhere (Zimmermann et al., 2004; Schmidt et al., 2020). The protocol uses a site-density based geostatistical procedure to identify Core Areas (CA; Schmidt et al., 2020), which represent clusters of archaeological sites, interpreted as continuously and permanently settled regions (Maier et al., 2016; Zimmermann et al., 2009). For an analysis such as ours, which covers a period of several thousand years, CA clustering appears to be an appropriate spatial up-scaling procedure for archaeological sites.. The CA comprised in total 310 archaeological sites across Europe.

We divided Europe along the 10°E longitude into a western and an eastern population (Fig. 1). Archaeologically, this division reflects the border between the Solutrean technocomplex to the west and the Epigravettian technocomplex to the east. The number of sites in Europe assigned to the western and eastern areas is given in Table 1.

2.2. Paleoenvironmental and paleoclimatic data

The climate data, basically temperature and precipitation, in this study were obtained from a 30-year regional climate simulation for LGM conditions (Ludwig et al., 2017) using the Weather Research and Forecasting (WRF) model (Skamarock et al., 2008). The WRF model was nested in the LGM run of the global earth system model MPI-ESM-P (Stevens et al., 2013), which was part of the Paleoclimate Modeling Intercomparison Project (PMIP3) (Braconnot et al., 2012). The WRF model used a much higher spatial resolution (50 km grid spacing) compared to the MPI-ESM-P (approx. 200 km) and thus provided more detailed information on the climate in Europe under glacial conditions. More details about the benefits of regional paleo-climate modeling are given in Ludwig et al. (2019). To take into account the glacial boundary conditions, the WRF model input data were modified in the extent and height of the Eurasian ice sheet, lowered sea level, and displaced

[2] https://crc806db.uni-koeln.de/dataset/show/crc806e1lgmsitesdatabase20150313142839605 9/.

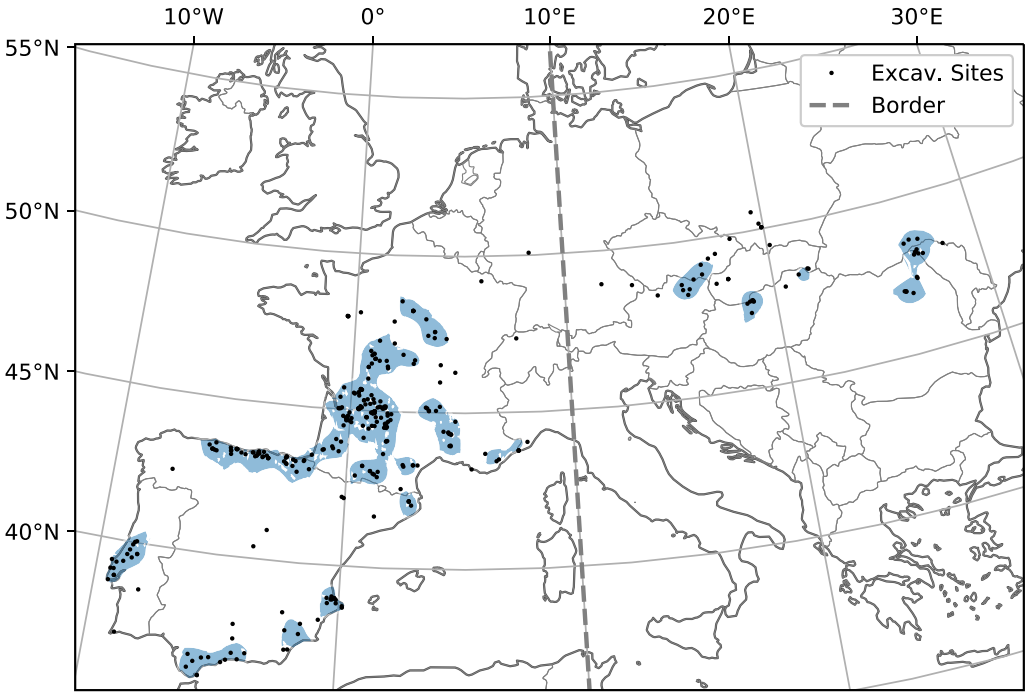

Fig. 1. Archaeological sites dated or assigned to the LGM (black dots, after Maier and Zimmermann (2015)), Core Areas are encircled by the "Optimally Describing Isoline" (blue shading, after Maier et al. (2016)) and the boundary between the western and eastern population (dashed gray line). (For interpretation of the references to color in this figure legend, the reader is referred to the Web version of this article.)

Table 1
The number of archaeological sites depending on the classification into the populations as shown in Fig. 1; (i) DatALL: all sites, (ii) DatCA: sites within Core Areas.

	Western Population	Eastern Population
DatALL	307	51
DatCA	278	32

coastline. These conditions were adjusted based on the PMIP3 protocol for LGM simulations. Finally, the paleo-vegetation data were obtained from a global vegetation reconstruction for the LGM from Shao et al. (2018). The paleo-vegetation reconstruction and the PMIP3 data were also used to determine the HEP accessibility described in Section 3.4.

3. Definition of the human existence potential

In general, humans are capable of adapting to various environmental conditions if food and water supply are ensured. Both resources are mainly controlled by temperature and precipitation. However, adaptation to certain environmental conditions may also prohibit humans from occupying all potentially inhabitable areas. Instead, they may prefer familiar environmental conditions and continue living under these if possible. Given this cultural selective factor, it is legitimate to use archaeological data to train the Human Existence Potential (HEP) on archaeological site distribution.

Four subsets of archaeological site data, as defined in Table 1, are used to model the HEP. We thereby distinguish between HEP derived by sites affiliated to the Solutrean technocomplex in western Europe ($\leq$10°E) and sites affiliated to the Epigravettian technocomplex in eastern Europe (>10°E); and DatAll sites (HEP_{ALL}), and DatCA sites (HEP_{CA}). The four different HEPs are west HEP_{ALL}, west HEP_{CA}, east HEP_{ALL}, and east HEP_{CA}. Given the interpretation of Core Areas, HEP_{CA} can be interpreted as representing the suitability of regions for continuous settlement for a given technocomplex. As the climate data is considered to represent the mean conditions of the LGM, we, furthermore, assume that HEP_{CA} reflects the mean HEP for continuous settlement. As DatALL includes archaeological outliers, i.e., sites that are considered to be only temporarily occupied, the difference $\Delta HEP = HEP_{CA} - HEP_{ALL}$ points to temporary variations from the mean conditions. In particular, negative ΔHEP regions were probably settled in intermittent phases of favorable climatic conditions.

The HEP is calculated by applying logistic regression with second-degree polynomials on a presence and absence record for suitable climatic predictors. The different bioclimatic predictors are derived by monthly mean temperature, daily maximum and minimum temperature, and monthly precipitation. The resulting HEP is a function of climatological predictors that presents the least to most desirable conditions for human existence with corresponding scores from zero to one. The resulting HEP is modified by functions based on topography, glacies, water bodies, and vegetation, to account for the accessibility. A description of the HEP model setup and the evaluation of the model is given in the next subsections and summarized in Fig. 2.

3.1. Variable selection

From the 19 different bioclimatic variables (Hijmans et al., 2005; O'Donnell and Ignizio, 2012), calculated using the WRF (Weather Research and Forecast) model output (see Table 2), the predictors for the logistic regression are chosen. A description of how the bioclimatic variables are computed is included in Section A in the Appendix. The variables Bio 8 and Bio 9 (Fig. A.1e and Fig. A.1f) are excluded from the analysis, because the regression coefficients did not converge due to strong temperature variations, in particular in Eastern Europe.

In a regression analysis, collinearity can cause errors in categorizing the importance of a predictor by overestimating the variance of the regression parameters (Dormann et al., 2013). A standard method in statistics to overcome this problem is the evaluation of the variance inflation factor (VIF; Alin, 2010). This factor estimates how much of the variance of a regression model is inflated in comparison to the same

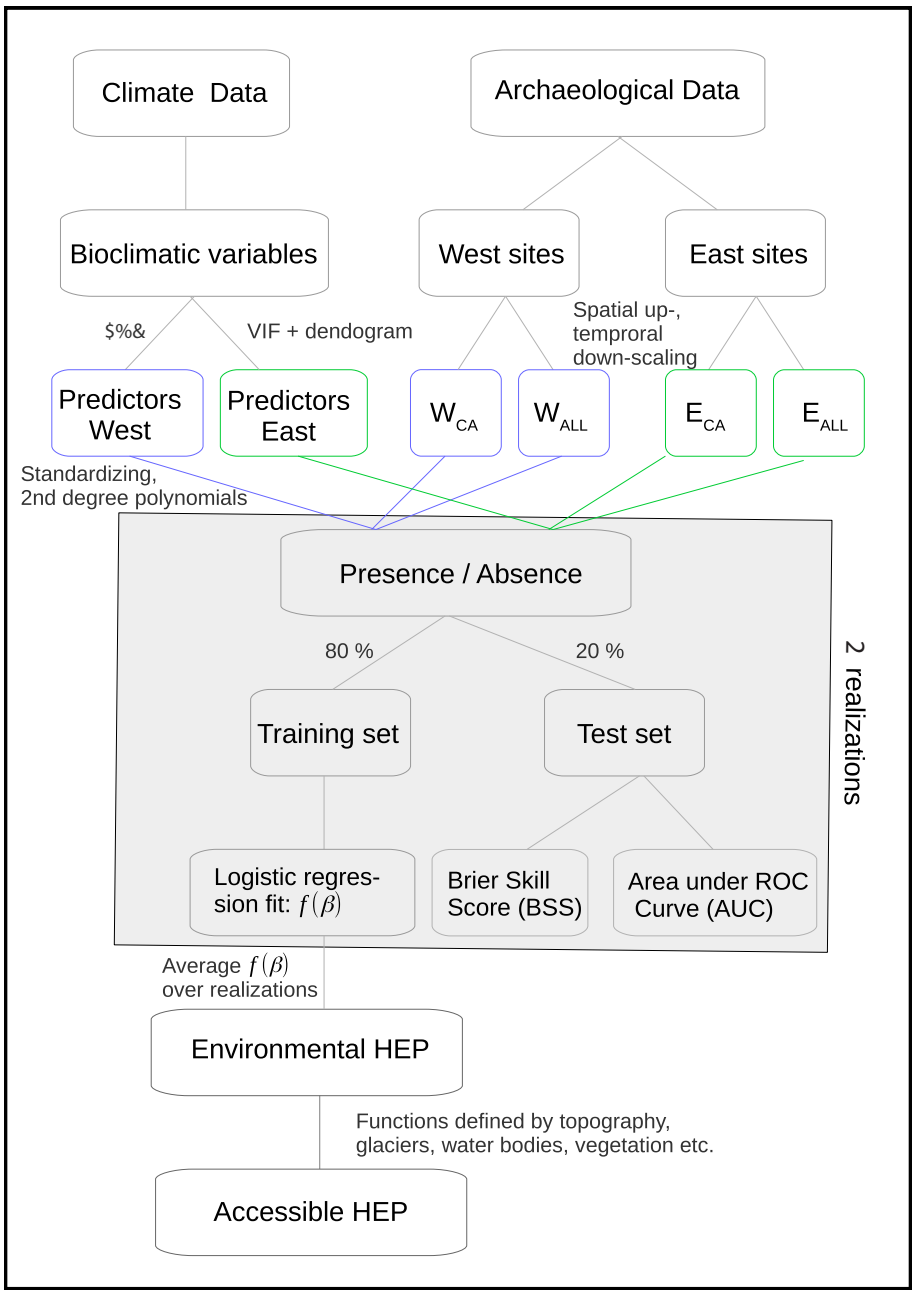

Fig. 2. Modeling framework of the Human Existence Potential (HEP).

model without collinearity. The VIF of each bioclimatic variable (b_i) is obtained by determining the Coefficient of Determination (R) from the ordinary least square regression with b_i as the predictand and the other bioclimatic variables as the predictors. The VIF of b_i is then:

$$\mathrm{VIF} = \frac{1}{1 - R^2}. \tag{1}$$

The VIF of each bioclimatic variable is required to be less than 10. We calculate the VIF of each variable and exclude the one with the highest VIF, except for Bio 4 or Bio 15, because both, namely the seasonality of temperature and precipitation, are known to be high impact predictors for the population of hunter-gatherers, as suggested by Grove (2018), and should be part of the analysis. We repeat the above step until the requirement (VIF < 10) is satisfied for all remaining variables. The distributions of the final seven variables used in the regression Bio 1, 3, 4, 14, 15, 18 and 19 are shown in Fig. 3.

The seven variables are used to estimate the HEP of the western population. For the eastern population, it is necessary to adjust the HEP model due to the low density and amount of archaeological sites (Table 1). The number of predictors have to be decreased to reduce errors from an under-parameterized model. We, therefore, further analyze the mutual correlations of the seven variables. The correlations are converted into a distance matrix by calculating the distance scores between two bioclimatic variables b_i and b_j with i, $j \in [1, 3, 4, 14, 15, 18, 19]$, by:

$$d_{i,j} = 1 - \left|corr(b_i, b_j)\right|, \tag{2}$$

while $corr(b_i, b_j)$ is the correlation coefficient between b_i and b_j. By joining two clusters of the resulting distance matrix into a single new cluster until one final node is left (Müllner, 2013), a hierarchical dendrogram correlation clustering can be drawn (Fig. B1). The distances between two clusters are the minimum distances between the corresponding variables. We choose a distance threshold of 0.3 to define the

Table 2
Definition of the 19 Bioclimatic variables as candidate predictors of the HEP. The corresponding definition for each of the variables is shown in the Appendix.

Bioclimatic Variable	Definition
Bio 1	Annual Mean Temperature
Bio 2	Mean Diurnal Range
Bio 3	Isothermality
Bio 4	Temperature seasonality
Bio 5	Max Temperture of Warmest Month
Bio 6	Min Temperature of Coldest Month
Bio 7	Temperature Annual Range
Bio 8	Mean Temperature of Wettest Quarter
Bio 9	Mean Temperature of Driest Quarter
Bio 10	Mean Temperature of Warmest Quarter
Bio 11	Mean Temperature of Coldest Quarter
Bio 12	Annual Precipitation
Bio 13	Precipitation of Wettest Month
Bio 14	Precipitation of Driest Month
Bio 15	Precipitation Seasonality
Bio 16	Precipitation of Wettest Quarter
Bio 17	Precipitation of Driest Quarter
Bio 18	Precipitation of Warmest Quarter
Bio 19	Precipitation of Coldest Quarter

main branches of the dendrogram, the largest (positive or negative) correlation between any two parameters from different branches is then in the range from −0.7 to 0.7. As already discussed, Bio 4 and Bio 15 are kept as predictors. In addition, Bio 1 is kept to retain the information of the temperature extremes. The extracted four variables, Bio 1, 4, 15 and 19, are used for modeling the HEP based on sites of the eastern population.

3.2. Model fitting

All climate variables are standardized by removing the mean ($\langle b_i \rangle$) and normalizing with the standard deviation (σ_{b_i}):

$$b_i^s = \frac{b_i - \langle b_i \rangle}{\sigma_{b_i}} \tag{3}$$

Second-order polynomials of the standardized climate variables are then used as predictors ($\vec{p}$) to fit the logistic regression (Eq. (4)).

The logistic regression model (Tibshirani, 1996; Hastie and Friedman, 2008) needs to be fitted with the human presence and absence records. Human presence is assumed in the circle with a 50 km radius centered at each archaeological site. The climate state at a grid point lying inside the circles is affiliated with the presence record, while each state is only once included to the record (total number: N_{pre}). A radius of 50 km is assumed, so that the number of presence points is sufficiently large for model convergence. The pseudo-absence record is assumed by the absence of archaeological sites in a region, and therefore consists of all grid points lying outside the circles (total number: N_{abs}). The pseudo-absence points for Italy and the Balkans are excluded to avoid false assumptions on human absence due to above mentioned constraints (Maier et al., 2016). Moreover, the climatic states for Africa, any islands, water bodies and areas north of 56°N are omitted from the analysis. The locations of presence (from eastern and western population combined) and absence points for DatALL are shown in Fig. 4.

We carry out 1000 calculations. For each, we randomly split 80% of the presence and 80% of the absence record into a training dataset, and the remaining 20% of both datasets into a test dataset. The coefficients $\vec{\beta}$ and the intercept β_0 are determined by the logistic function of the training data:

$$y_i^{train} = \left\{1 + \exp\left[-\left(\beta_0 + \vec{\beta}\cdot\vec{p}_i^{\,train}\right)\right]\right\}^{-1} \tag{4}$$

with $y_i^{train} = 1$ for presence and $y_i^{train} = 0$ for absence points, for $i = 1,\ldots, 0.8\cdot(N_{pre} + N_{abs})$. The presence and absence input are weighted by the amount of presence and pseudo-absence points, respectively. The logistic regression involves 36 terms for the western and 15 terms for the eastern population, but not all terms are important. For that, LASSO (Least Absolute Selection and Shrinkage Operator) regularization (Tibshirani, 1996; Hastie and Friedman, 2008; Marami Milani et al., 2016) is used in the training process to exclude irrelevant terms of the polynomials.

The trained model (f) is then applied to the whole study area and the averaged outcome over the 1000 realizations is the HEP for Europe.

$$\begin{aligned} \mathrm{HEP} &= \tfrac{1}{1000}\textstyle\sum_{j=1}^{1000} f_j(\vec{p}) \\ &= \frac{1}{1000}\sum_{j=1}^{1000}\left\{1 + \exp\left[-\left(\beta_{0,j} + \vec{\beta}_j\cdot\vec{p}\right)\right]\right\}^{-1} \end{aligned} \tag{5}$$

3.3. Model evaluation

The test dataset is applied for cross validation. Different skill scores are determined to evaluate the uncertainty of the model, where the prediction $f(\vec{p}^{\,test})$ of each realization is compared to the classification $\vec{y}^{\,test}$ (1 for presence and 0 for absence). The "Area under a Receiver Operating Characteristics Curve" (*AUC*) is determined to estimate the rate of cases which the method classifies correctly (Hanley and McNeil, 1982). The AUC values range from 0 to 1, while 0 means that all predictions are classified wrongly and 1 that all predictions are classified correctly. The Brier Score for each of the 1000 realization is calculated by:

$$BS = \frac{1}{N_{test}}\sum_{i=1}^{N_{test}}\left(f\left(\vec{p}_i^{\,test}\right) - y_i^{test}\right)^2 \tag{6}$$

with $N_{test} = 0.2\cdot(N_{pre} + N_{abs})$. By comparing the Brier Score of the trained model (BS_f) with the Brier Score of the same model where all coefficients except the intercept are set to zero (BS_{β_0}), the Brier Skill Score (*BSS*) can be estimated to measure the accuracy of a model:

$$BSS = 1 - BS_f / BS_{\beta_0} \tag{7}$$

The mean and the standard deviation of BSS and AUC of all 1000 realizations are calculated. In addition, the total variance (Var) of the 1000 predictions ($f(\vec{p})$) is computed to get a measure of the robustness of the output according to the input data. The results of the evaluation for all four model setups are shown in Table 3.

For all four subsets of archaeological site data, the model shows robustness to the input variables, as indicated by the low total variances shown in Table 3. Sensitivity analysis (Fig. D.1 in the Appendix) shows that local variances are generally low despite a few regions, e.g. the Pyrenees. The relatively high local variances are probably due to the inclusion of climatological outliers into the presence record. Both BSS and AUC suggest that model prediction work properly for all four setups (Table 3). As both AUC and BSS show low standard deviations, we suppose that the model output differs only marginally for different random setups. Thus, we suppose, that the occurrence of new archaeological findings would have only minor and rather local effects on the resulting HEP.

3.4. Accessibility

The HEP covers the main climate factors influencing the habitability, but the accessibility of resources is not considered. To account for important limiting factors such as orography and water bodies, several functions are introduced to modify the HEP. The result (HEP_{Acc}) is still referred to as HEP in the following discussions (Eq. (8)).

$$\mathrm{HEP}_{Acc} = \mathrm{HEP}\cdot g_{ice}\cdot g_{ele}\cdot g_{for}\cdot\ldots \tag{8}$$

The modification functions, unless stated otherwise, are linear functions of the structure depicted in Eq. (9), with the input variable x,

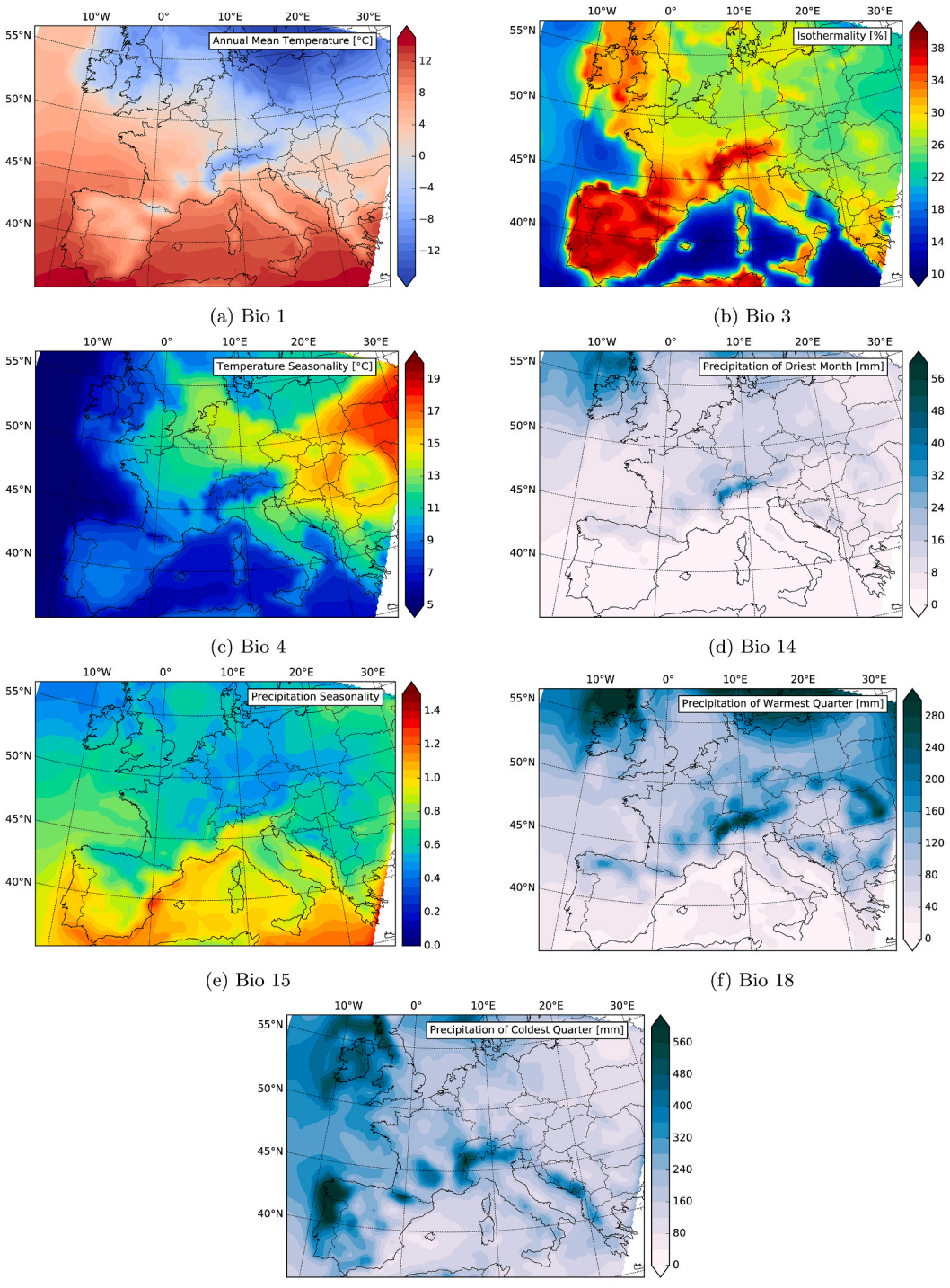

(a) Bio 1 (b) Bio 3

(c) Bio 4 (d) Bio 14

(e) Bio 15 (f) Bio 18

(g) Bio 19

Fig. 3. Climate maps of the seven predictors used to calculate the Human Existence Potential (HEP).

the upper and lower limits x_u and x_l, and the slope m between the limits. Each modification function can diminish the HEP by up to 20% if the upper limit is reached. The empirical chosen parameters are listed in Table 4.

$$g(x)_{par} = \begin{cases} 1.0, & x < x_l \\ 1.0 - (x - x_l)\cdot m, & x_l \leq x < x_u \\ 0.8, & x \geq x_u \end{cases} \quad (9)$$

3.4.1. Ice, glaciers and water bodies

The permanent presence of sea ice and glaciers act as natural barriers for hunter-gatherers. As no vegetation or wildlife is in these areas to sustain humans, the HEP is set to zero. Natural water bodies such as oceans and large lakes act as impassable borders and are masked out. We use the PMIP3 reconstruction of the glaciers and the LGM coastline (Braconnot et al., 2012).

$$g_{water,ice} = \begin{cases} 0, & \text{if gridpoint is water or ice} \\ 1, & \text{otherwise} \end{cases} \quad (10)$$

3.4.2. Orography

A crucial limiting factor of available resources is the orography. In

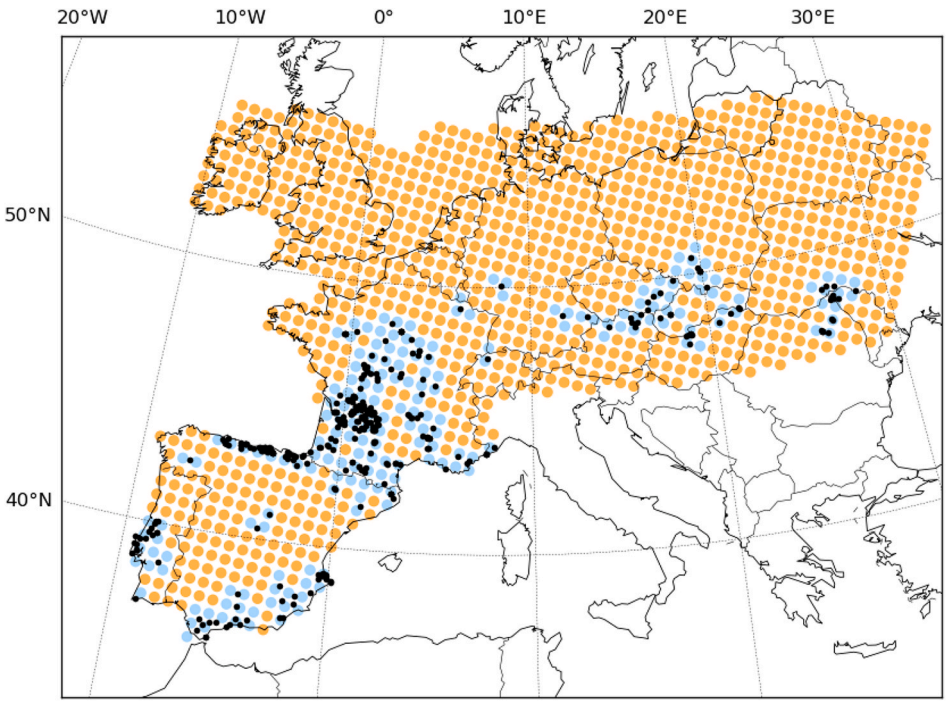

Fig. 4. Black dots: archaeological sites of DatALL (eastern and western sites combined) according to Table 1 across Europe. The underlying presence (blue) and pseudo-absence points (orange) for the calculation of the HEP are depicted. (For interpretation of the references to color in this figure legend, the reader is referred to the Web version of this article.)

Table 3
Mean and standard deviation of Area under a Receiver Operating Characteristics Curve (AUC) and Brier Skill Score (BSS) for the 1000 realizations, and total variance of the 1000 realizations (Var) of the prediction f, derived by the model setups W_{CA}, W_{All}, E_{CA} and E_{All}.

	W_{CA}	W_{All}	E_{CA}	E_{All}
AUC	0.94± 0.02	0.94 ± 0.02	0.95 ± 0.03	0.93 ± 0.02
BSS	0.6± 0.05	0.56 ± 0.05	0.63 ± 0.05	0.54 ± 0.06
Var	0.02	0.013	0.001	0.001

Table 4
List of parameters used in each modification function.

Parameterization	Variable x	Slope m	Lower limit x_l	Upper limit x_u
Elevation g_{ele}	h	$0.1212{\cdot}10^{-3}$	350 m	2000 m
Standard deviation of elevation g_{std}	h_σ	$0.5714{\cdot}10^{-3}$	50 m	400 m
Vegetation g_{for}	f_f	0.4	0.5	1

complex terrains (such as mountains, valleys, and cliffs), topographic obstacles make hunting and gathering more difficult so that the accessibility of resources is reduced in these regions. However, some complexity may be more favorable than flat terrain to find shelter, raw materials for tools and a higher diversity of resources. The elevation and complexity of the landscape are taken into account to evaluate the orographic influences.

Histograms (Fig. C.1 and Fig. C.2, see appendix) of the elevation of sites and the standard deviation of the elevation around the sites are created using a 30 s topography dataset. The standard deviation is used to estimate the roughness of the terrain in a grid cell of the climate data. The ordinate shows the normalized number of site bins of 50 m width (10 m width for standard deviation). Fig. C.1 shows that elevations (h) of 200 m–300 m are more frequent, while sites with higher altitudes are less frequent. We set the interval for the HEP decline from 350 m to 2000 m. For the standard deviation (h_σ), the terrain featuring variations above 50 m is less occupied than nearly flat terrains. A low number of sites are found near high altitude variations. The boundaries are set to 50 m and 400 m to formulate g_{std}.

3.4.3. Forest and dense vegetation

Dense vegetation makes the transport more difficult while gathering, hunting or dispersing. We assume that areas with a large forest cover were less favorable. Humans could still survive in dense forests, but plant based foods are less accessible, e.g. higher up in the canopy or within the thicket (Kelly, 2013; Binford, 2002). We apply the global vegetation reconstruction of the LGM from Shao et al. (2018), focusing on the forest fraction. The potential is not altered for a forest fraction (f_f) below 0.5. For larger fractions, the potential is lowered with a linear function starting at 0.5 and ending at 1 for a full forest cover.

4. Best Potential Path and Environmental Human Catchment

We estimate BPP using a similar method as in Kondo et al. (2018). For a given grid, a cost function, C, is defined as 1/HEP (for HEP $\leq 10^{-5}$, C is set to 10^5). The total cost T between points A and B along a path s is:

$$T = \int_A^B C\, ds, \tag{11}$$

while we scale the distance between two grid points by $1/100\ km^{-1}$. From all possible paths between the two points, the BPP is the one of the lowest T, referred to as T_{BPP}. We compute the exchange network of the Solutrean technocomplex by determining the BPPs between the adjacent Core Areas.

To determine the EHC, we first extract catchments from the HEP pattern by identifying the local maxima and determining the associated upflow of each grid point to the maxima. By our definition, only catchments with a local maximum greater than 0.85 are specified as an EHC. We implement several rules so that catchments with lower maxima

merge into more substantial neighbouring catchments if they are not separated by low HEP < 0.5. Also, two EHCs with a direct transition are combined. The decision tree is shown in Fig. 5 and explained as follows:

1. If the HEP of the local maximum of a catchment (HEP_{LM}) is less than or equal to 0.85, it is surveyed if an adjacent catchment is an EHC ($HEP_{LM} > 0.85$). If yes, the catchment is merged with the EHC if they have more than two adjacent grid points with HEP > 0.5. If two or more adjacent catchments are EHCs, the catchment is merged into the one which has the lowest the minimum difference between the adjacent grid points.
2. Two adjacent EHCs are merged, if there are adjacent grid points with HEP ≥ 0.8.

We repeat these steps ten times to capture all catchments which would merge. The resulting catchments satisfying $HEP_{LM} > 0.85$ are the EHCs.

5. Results

We estimate the HEP using either DatCA or DatALL and denote the results respectively as HEP_{CA} and HEP_{ALL}. While HEP_{CA} describes as reference the time averaged potential during the LGM, which enables continuous human occupation, the difference $\Delta HEP = HEP_{CA} - HEP_{ALL}$ provides insights in the potential variations which allow intermittent human occupations. In order to investigate the separation between the Solutrean and Epigravettian technocomplexes, HEP_{CA} and HEP_{ALL} are computed individually for western and eastern Europe. In the following, the HEP results are first described and then the BPP and EHC results. To facilitate discussion, regions with HEP ≥ 0.5 are referred to as high HEP regions.

5.1. Western population

For the population in western Europe, or simply western population, the highest HEP_{CA} are located in the Franco-Cantabria with values exceeding 0.9 throughout the region (Fig. 6a). On the Iberian Peninsula, HEP_{CA} shows suitable conditions along the northern, southern and southeastern coasts (e.g. $HEP_{CA} \geq 0.7$), but generally unsuitable conditions in the northwestern and central parts. The great mountain ranges in Europe, such as the Alps, the Pyrenees and the Massif Central in France are generally unfavorable for LGM hunter-gatherers with low HEP_{CA}, as expected. Outside the known regions of the Solutrean technocomplex, potential refugia with high HEP_{CA} occur in Italy and the Balkans, although the archaeological sites in these areas are excluded in the model training process (see Sec. 2.1). The regions with high HEP_{CA} east of Italy calculated using the model setup W_{CA} are exclusively located along the Mediterranean coast.

The spatial patterns of HEP_{ALL} (Fig. 6b) and HEP_{CA} partially differ. The most obvious differences occur in the inland regions of the Iberian Peninsula, northwestern Europe, and the Balkans (Fig. 8a). Clear differences can be seen in the Iberian Peninsula interior where HEP_{CA} is much lower than HEP_{ALL}. Similarly, high differences are observed at the northern and eastern margins of western Europe: high HEP_{ALL} regions extend to the northern border of France and southern parts of Great Britain, while high HEP_{CA} regions are confined more to the southwest. The upper Rhine rift valley, between southwestern Germany and France, has the largest ΔHEP. The highly suitable living conditions reflected in HEP_{ALL} almost entirely disappear in HEP_{CA}. The maximum ΔHEP here reaches around -0.5 (Fig. 8a). In eastern Europe, an increase can be observed for HEP_{CA} along the Adriatic Coast, while values for the hinterland conspicuously decrease. In Italy, the comparison shows higher HEP_{CA} in the Po valley, and lower values for the central region (Fig. 8a).

5.2. Eastern population

For the population in eastern Europe, or simply eastern population, HEP_{CA} indicates favorable living conditions around the Core Areas and some areas in Germany, the Czech Republic, and the Balkans (Fig. 7a). The highest HEP_{CA} of 0.97 is located in northeastern Hungary. The pattern is interrupted by low HEP_{CA} related to topographic features such as the High Tatras and the Carpathian Mountains. In northern Germany, there is an apparent mismatch between HEP_{CA} and the archaeological record, repeatedly reported in the literature (e.g., Maier et al., 2016). Interestingly, evidence of human presence (cf. archaeological sites in Fig. 7b) fits well with the southern boundary of HEP_{CA}-area in southern Germany (Fig. 7a).

The HEP_{ALL} shows high HEP regions in a rather continuous band stretching from the Netherlands to Moldavia in the east, and from the edge of the Scandinavian ice sheet to the northern Balkans in the south (Fig. 7b). The HEP_{CA} displays a less homogeneous pattern and a shrinkage of the western (i.e. Netherlands, Germany and western Poland) and northern extent of the band. The ΔHEP in Fig. 8b reveals the striking decrease of the HEP in these areas. Especially at the edge of the Scandinavian ice sheet, the HEP_{CA} deviates considerably from HEP_{ALL}, with a difference of up to 0.64. The pattern of ΔHEP in Fig. 8b shows positive values in regions in eastern Europe stretching from 46° to 48°N and negative values north and south of it.

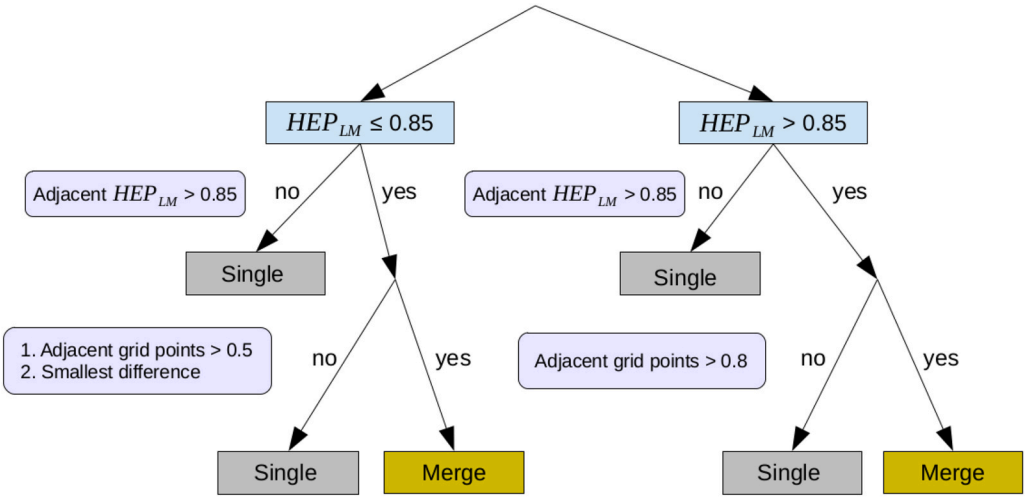

Fig. 5. Decision tree to illustrate when catchments are merged together. $HEP_{LM} > 0.85$ is the local maximum of HEP of the catchment.

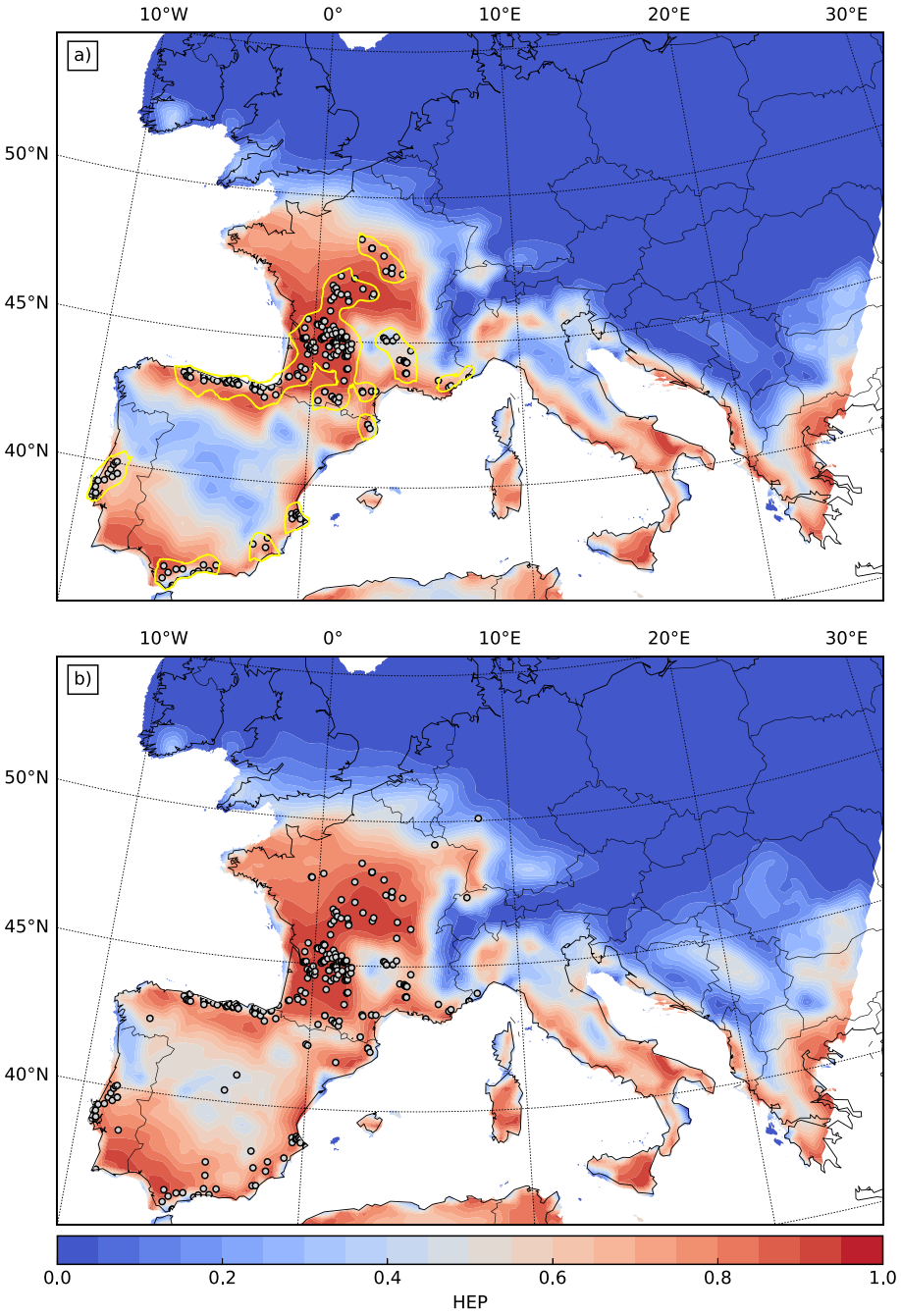

Fig. 6. Human Existence Potential (HEP) derived by logistic regression with the bioclimatic variables Bio 1, Bio 3, Bio 4, Bio 14, Bio 15, Bio 18 and Bio 19 and archaeological sites of the western population (west of 10°E). Thereby we incorporated for a) HEP_{CA} sites from Core Areas (DatCA) indicated by yellow lines, and for b) HEP_{ALL} all sites (DatALL). Gray dots: archaeological sites assigned to the LGM and incorporated in the model. (For interpretation of the references to color in this figure legend, the reader is referred to the Web version of this article.)

5.3. Application of the Best Potential Path to LGM Core Areas

We use BPP to investigate possible routes of the Solutrean social network across western Europe. To this end, we examine the BPP between Core Area centres in western Europe which are more than three grid points apart from each other. We provide two scenarios by calculating the BPP based on either HEP_{CA} (Fig. 9a) or HEP_{ALL} (Fig. 9b) of the western population with a total of 12 pairs of starting and ending points. Thereby, the BPP estimates how the social network of hunter-gatherers might have changed in intermittent phases of climate amelioration (considering HEP_{ALL}) in comparison to the continuous LGM conditions (considering HEP_{CA}). We arrange the total costs of the BPP (T_{BPP}) in five categories to get an estimate of the proximity of contact.

For both scenarios, the same distribution of BPPs is found between the Core Area centered in the Dordogne and the Core Areas in northern France, Cantabria and Catalonia. This stable pattern is corroborated by the low costs of the BPPs ($T_{BPP} < 6$). Contact between these Core Areas is expected to have been intensive and stable. The BPPs connecting the Rhône valley with Franco-Cantabria and Catalonia run along the coast and the low T_{BPP} indicate a stable contact between these Core Areas. While the cost of BPP between the north of France and the Rhône valley reaches to $T_{BPP} > 9$ considering HEP_{CA}, the cost sinks when considering

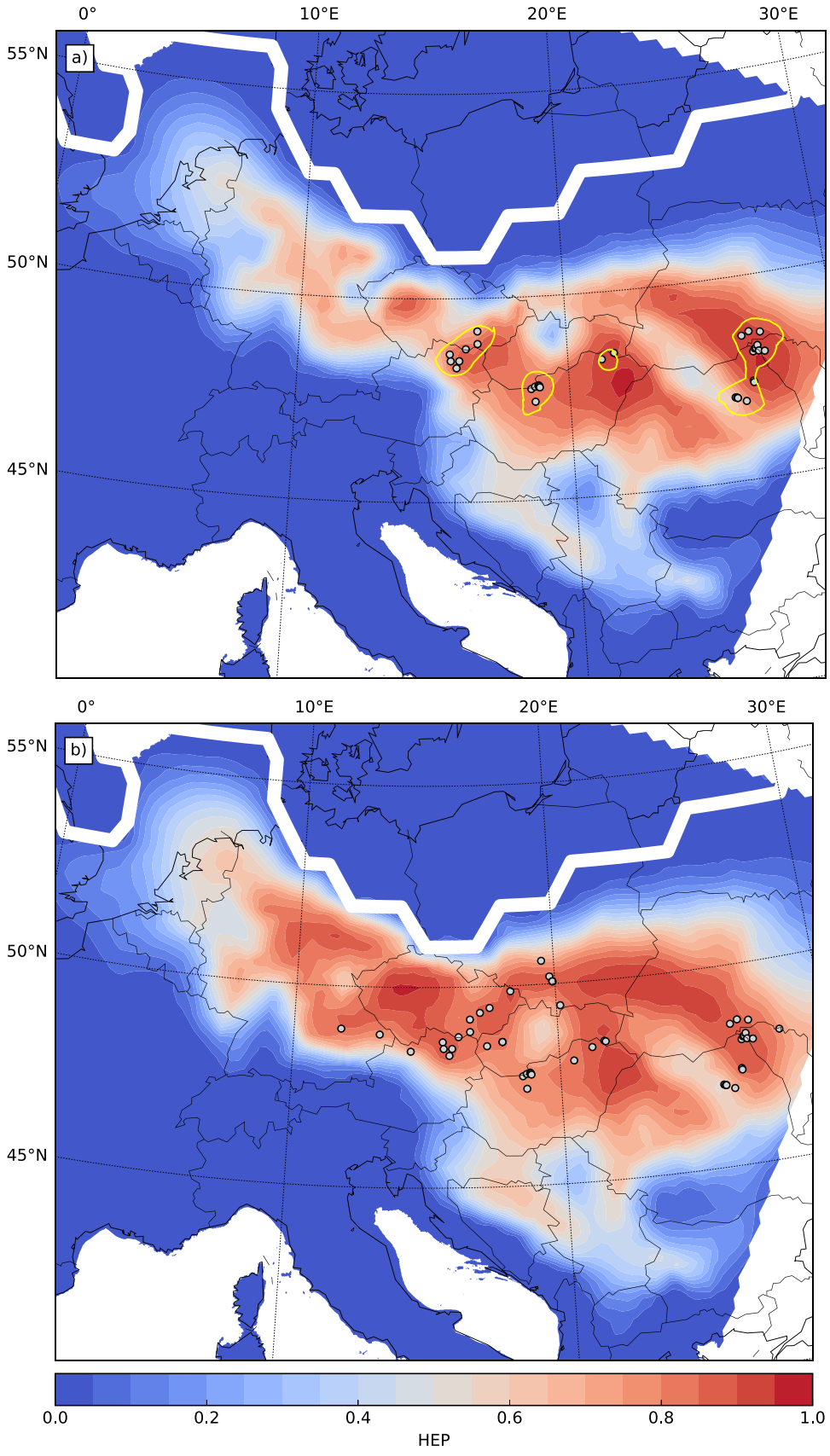

Fig. 7. Human Existence Potential (HEP) derived by logistic regression with the bioclimatic variables Bio 1, Bio 4, Bio 15 and Bio 19 and archaeological sites of the eastern population (east of 10°E). Thereby we incorporated for a) HEP_{CA} sites from Core Areas (DatCA) indicated by yellow lines, and for b) HEP_{ALL} all sites (DatALL). Gray dots: archaeological sites assigned to the LGM and incorporated in the model, white line: glacier extent from PMIP3-reconstuctions. (For interpretation of the references to color in this figure legend, the reader is referred to the Web version of this article.)

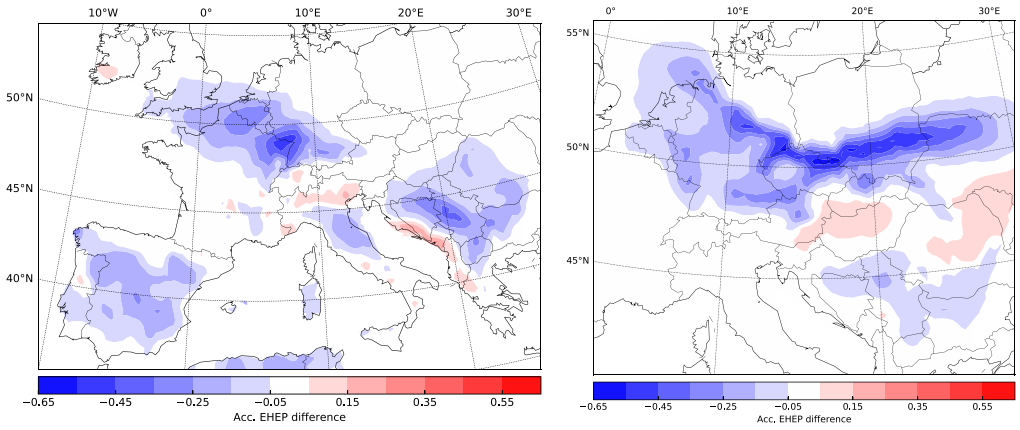

(a) (b)

Fig. 8. Difference between the HEP derived using sites from Core Areas (HEP_{CA}) and the HEP derived using all sites (HEP_{ALL}): $\Delta HEP = HEP_{CA} - HEP_{ALL}$; for a) the western population, and b) the eastern population.

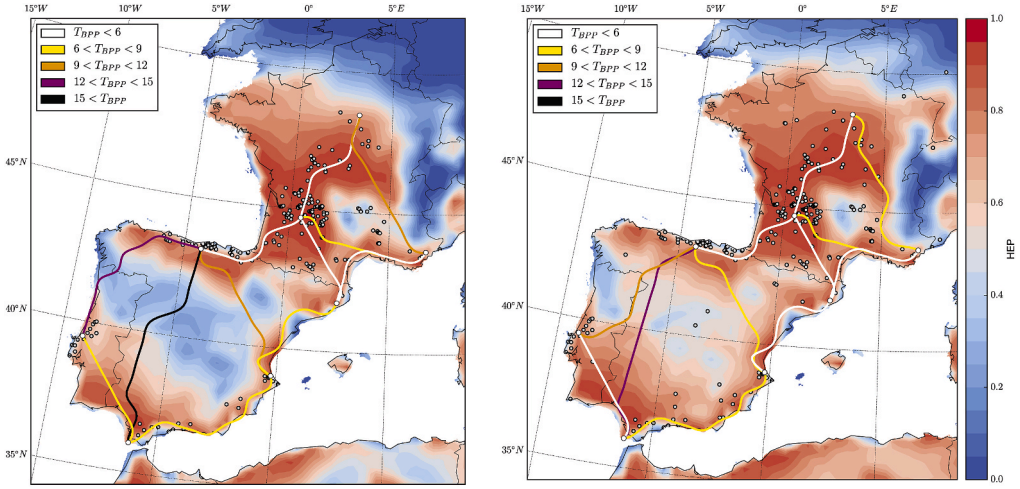

(a) (b)

Fig. 9. Solutrean social networks across western Europe established by computing the BPP between centres of Core Areas. The BPP is derived by either (a) using HEP_{CA} or (b) using HEP_{ALL}. The cost of the BPP (T_{BPP}) is indicated by the color. Gray dots: archaeological sites incorporated in the HEP model. (For interpretation of the references to color in this figure legend, the reader is referred to the Web version of this article.)

HEP_{ALL}. The BPP then crosses the Core Area at the Massif Central.

On the Iberian Peninsula, BPPs between the Core Areas located at the Mediterranean coast follow the course of the coastline, and for both scenarios the connections have relatively low costs ($T_{BPP} < 9$). The two BPPs going through the inland of Iberia, in contrast, display much higher costs, which are, however, somewhat lower if the BPPs are determined based on HEP_{ALL}. The BBP connecting the Core Areas between the north coast and the west coast of Iberia is associated with high cost based on the HEP_{CA} ($T_{BPP} > 12$). With HEP_{ALL}, the course of the BPP moves further inland, along the Vale de Côa, and the cost is lower.

5.4. Environmental Human Catchment

To evaluate the HEP for Europe as a whole during the LGM, we combine the HEPs of the western and eastern population into a single pattern. Since the high HEP regions of the western and eastern populations do not overlap (cf. Figs. 6 and 7), we take at each grid point the largest HEP_{CA} for either the eastern or the western population (Fig. 10). Next, the EHCs of the combined HEP_{CA} are identified by using the rules outlined in Fig. 5 and described in Sec. 4. In total, 15 EHCs are identified in Europe, with 12 associated with the western population and 3 associated with the eastern population (Fig. 10).

The biggest EHC of the western population comprises most parts of France and stretches from the south of Great Britain to the northwest of the Iberian Peninsula. It includes the Core Areas in Franco-Cantabria and northern France, and nine maximums with HEP > 0.85 (here after referred to as high local maxima). An EHC, incorporating the Rhône valley's, Catalonian and Massif Central's Core Area, is located along the Mediterranean coast. The Iberian Peninsula is separated into four additional EHCs, one covering the southwestern part and three dividing

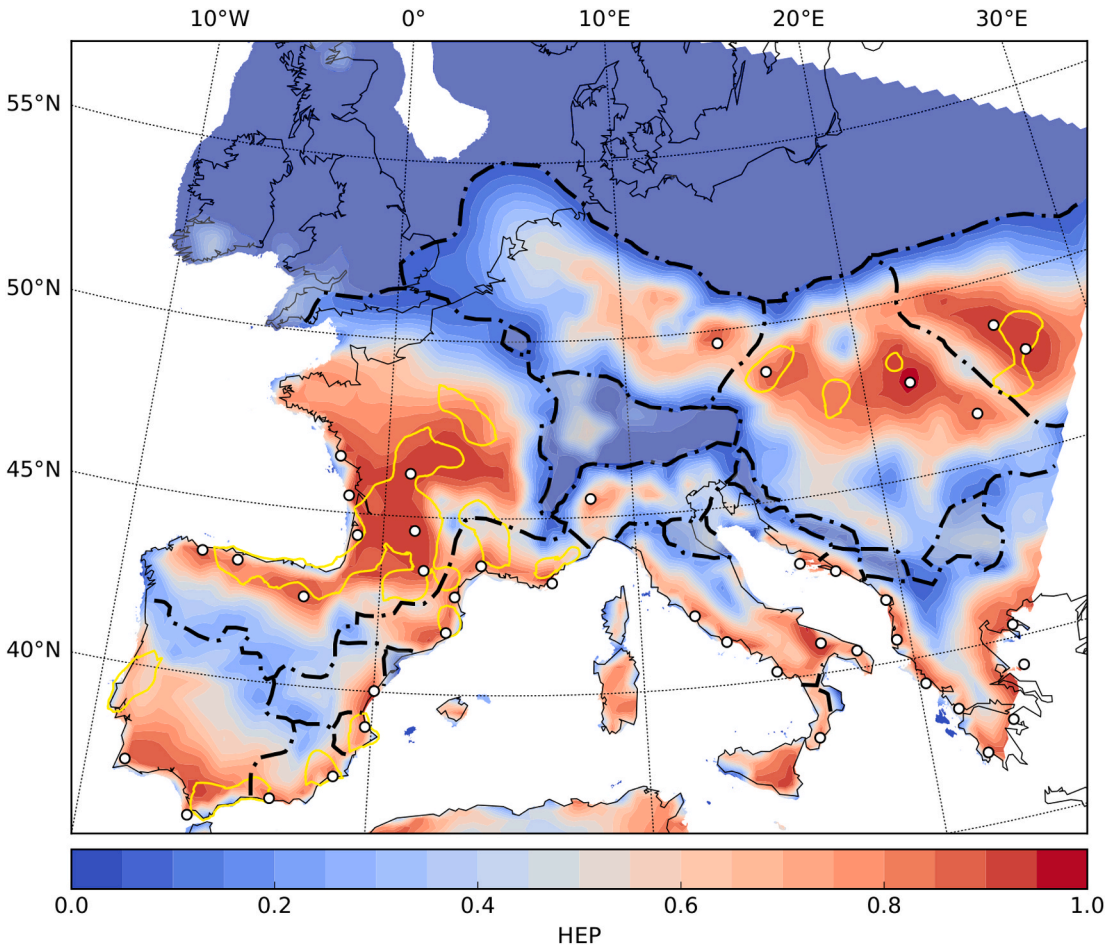

Fig. 10. Human Existence Potential (HEP) for Europe by selecting the largest HEP_{CA} of either the western or the eastern population (Figs. 6b and 7b). Environmental Human Catchments (EHC) are depicted by the black chain line. They are enclosed areas with HEP > 0.85 (white dots) and an "upflow" from each grid point to a local maximum. The rules applied to determine EHC are given in Fig. 5. Regions not belonging to an EHC are shaded.

the southeastern part. It is interesting to note that, apart from the high local maximum in Cantabria, all other high local maxima in Iberia are located along the coast. The HEP pattern in Italy and the Balkans is subdivided into a number of small EHCs, with high local maxima along the Mediterranean coast. The relatively sharp boundary dividing the EHC in northern Italy from the south may indicate that hunter-gatherers encountered environmental barriers hindering the southward expansion.

The eastern population considered in this study is divided into three EHCs. The westernmost EHC includes four minor catchments in the Netherlands and Germany, while the maximum, with a HEP of 0.87, is located in the Czech Republic. The maximum of one of the EHCs further east is in Hungary. It extends to the southern regions, bordering with the eastern EHCs associated to the western population. The other EHC covers the northern parts of the high HEP regions with a possible extension to areas further east, which are not included in our dataset.

6. Discussion

The presented HEP results show that the spatial up- and temporal down-scaling of archaeological data provides new insight into the settlement patterns of hunter-gatherers during the LGM. Mismatches between the archaeological record and the model, or differences between the HEP derived on different datasets (i.e. here DatALL and DatCA) are useful to enrich our understanding of human adaptation. While both, HEP_{CA} and HEP_{ALL}, agree well with the archaeological records for regions of high site density, HEP_{CA} better coincides with the records for regions where none or low presence of hunter-gatherers was expected. For example, while both high HEP_{CA} and HEP_{ALL} regions cover Franco-Cantabria, HEP_{CA} is smaller than HEP_{ALL} in Central Germany and inland Iberian Peninsula, which were sparsely populated based on archaeological evidence.

Fig. 10 shows that 33% of the land area has a HEP_{CA} (eastern and western HEP_{CA} combined) larger than 0.5, and 59% larger than 0.1. These percentages correspond to the minimum and maximum percentages of inhabited land areas estimated by Tallavaara et al. (2015), who investigated human population dynamics from the pre-LGM at 30 ky to the Late Glacial at 13 ky in Europe using modern ethnographic population densities and climate envelope modeling. This outcome indicates that during the LGM high HEP_{CA} regions were inhabited during harsh climate and new territories were explored when the climate became more favorable.

A significant negative ΔHEP is found at the extent of the glacier based on the eastern setup and in the northeastern part of France and northern part of the Balkans for the western setup. This outcome suggests that hunter-gatherers settled continuously in more southern latitudes during the LGM, while intermittent settlements were possible further north. The occurrence of archaeological sites north of the high HEP_{CA} regions can be explained by temporal excursions either under stable conditions or - more likely - during phases of climatic amelioration. Negative ΔHEP also occurs in inland Iberian Peninsula. HEP_{CA} is much lower in the inland than along the coast, indicating that only the coastal areas of the Iberian Peninsula provided stable conditions for viable populations, a long-standing and intensively debated pattern (see Alcaraz-Castaño et al., 2019). ΔHEP suggests that changing climate conditions have increased the probability of hunter-gatherer settlements in the inland in intermittent phases.

The HEP pattern in the Iberian Peninsula is also reflected in the BPP analysis of the Solutrean social network: the cost of the BPP is the lowest along the coast (see Weniger et al., 2019). However, the cost of inland BPPs decreases using HEP_{ALL}, suggesting that changing climate provided intermittent corridors for social networks among hunter-gatherers. These corridors provide plausible explanations to the existence of archaeological sites in inland Spain, such as Peña Capón in the central area and sites of Foz Côa along the north-western route. An improved insight into the social network can be achieved by using higher resolution climate data or by incorporating variables important on smaller time and spatial scales, such as the perceived accessibility and the perception of the landscape.

A striking result of our study is that areas of high HEP_{CA} do not overlap for the eastern and western population. A pattern that is also reflected in the EHCs which are clearly separated for the eastern and western populations. These results suggest that the two population groups inferentially adapted to different environmental conditions and that an environmental barrier may have divided the two groups and prohibited interactions between them. This finding appears to explain the emergence and persistence of the Solutrean and Epigravettian techno-complexes in western and eastern Europe, respectively, throughout the LGM. In comparison to Maier et al. (2016), who came to the same conclusion, our results show a more pronounced difference of environmental adaptations. Possible changes to these observations might emerge when Italy and the Balkans are considered in the training process of the HEP. However, the current reconstructions of the environmental conditions do not support the narrative that close contact between the two populations existed during the LGM. A southward orientation of movement within the Epigravettian is nevertheless possible as suggested by the negative ΔHEP in the Balkan region, which are located to the South of the currently considered eastern European sites.

The EHCs reflect patterns of internal regionalization within the techno-complexes during the LGM. These patterns show a tight correlation with the distribution of regional variants of Solutrean point types on the Iberian Peninsula, which emerged during the Middle and Late Solutrean. These point types, reflecting regional traditions of point manufacture, use, and stylistic - or even idiosyncratic - expressions (Schmidt, 2015a, b), have already been related to ecological niches (Banks et al., 2009). The EHCs underpins the likeliness that these groups would be attracted to the environmental catchments. New studies comparing the extent of EHCs with regional traditions could lead to interesting results.

Exploring the relation between large-scale patterns of human distribution and environmental factors relies heavily on our understanding and the robustness of the model. Noticeable mismatches between the HEP and the archaeological records exist in some areas. For example, high HEP regions are simulated in central Germany and the Netherlands based on sites of the eastern population, although no archaeological sites have been found there. There are several likely reasons for this mismatch. First, the density of the eastern population was not large enough to trigger dispersal by population pressure. This explanation is supported by the pattern of the EHC. Given the definition of an EHC, preceding external drivers would be required for the eastern population to explore western parts of Germany. As there were no archaeological sites assigned to the LGM in these regions, it is likely that such drivers did not exist. This observation is in accordance with the finding of Maier et al. (2016), that the population density in eastern Europe was extremely low, probably too low to act as a driving force for human emigration out of the catchment into areas further west. It is also likely that since predictors such as flora and fauna, which were only taken indirectly into account in our study by the bioclimatic variables, change the HEP if they are considered. However, adding additional predictors to the model can cause uncertainties on larger scale. Nevertheless, the exclusion of relevant predictors or inclusion of irrelevant predictors is a possible explanation for the mismatches between the modeled HEP and archaeological records. The possibility of archaeological biases, i.e., remains have either not been found or vanished over time, seems rather unlikely, given the current state of knowledge of these regions. Furthermore, as we showed in section 3.3, the HEP model is robust to new archaeological input data.

Another reason for mismatches is probably related to the resolution of the environmental dataset: conspicuously low HEP - despite the presence of several archaeological sites - are observed for the western population at the Massif Central. This area could have been explored and inhabited by hunter-gatherers in intermittent phases of climatic change. Valleys, which are beyond the spatial resolution of our datasets, might have provided niches for temporal or even continuous settlement along the mountains. Better insights of the HEP can be provided in the future by increasing the spatial resolution of the climate data (e.g., Burke et al., 2017; Ludwig et al., 2018).

The 30-year climate simulation which is assumed to represent the average conditions during the LGM from 25 to 20 ky BP, is based on steady state conditions with constant orbital parameters and greenhouse gas concentrations, as evaluated for 21 ky BP, and with a fixed glacier extent and constant surface conditions. This assumption is certainly not the full truth, as changing external forcing must have influenced the climate during the 5000 year period, so that the long-term climate changed. More realistically would be a time dependent HEP(t) for the LGM based on changing climate conditions. Especially the margins of the high HEP_{CA} regions could have extended northwards during warmer and shifted southwards during colder conditions.

7. Conclusion

In this study, we investigate the human existence potential (HEP) and its implications for human movement and interactions on regional to continental scales in Europe during the LGM. The HEP is evaluated by applying logistic regression of bioclimatic predictors to a dataset of human-presence and -absence based on archaeological sites. The concept of HEP defines the upper limit of the resources available to humans given the technological structure and the social development of the humans. To account for the accessibility, the HEP is computed by applying modification functions, which depend on topography, glaciers, water bodies, and vegetation. By integrating temporal up-scaled

archaeological site data into the HEP model, we could identify regions continuously habitable for humans during the LGM and regions habitable in intermittent phases of climatic improvement. We could thereby explain some of the earlier mismatches between models and archaeological records. We show that, while inland Iberia and regions close to the Scandinavian Ice Sheet were areas unfavorable for continuous settlement in the LGM, those areas had high HEP in intermittent phases, which provided suitable conditions for human settlement, aligning with the sporadic occurrence of archaeological sites.

Due to the harsh climate conditions at the time, most regions in Europe were uninhabitable, only for 33% of the European mainland did the HEP exceed 0.5. This constriction of suitable habitats must have affected the mobility and cultural and demographic developments of humans. Our results support the hypothesis of a human population breakdown in parts of central Europe during the LGM as reflected by the limited inhabitable area, continuing the developments of the final Gravettian. The results also indicate that the western and eastern populations adapted to different environmental conditions, supporting the hypothesis that the emergence and persistence of the Solutrean and Epigravettian techno-complexes in western and eastern Europe, respectively, throughout the LGM were driven by the environment. Moreover, we show that an environmental barrier probably prevented the contact between the two populations.

The BPP and EHC study help to improve our understanding of the dynamics and regionalization of hunter-gatherers, and the social and technological interactions between them. The EHC classification indicates the separation of Solutrean and Epigravettian hunter-gatherers during the LGM. Also, the EHC patterns allow the identification of areas of internal regionalization, as for example on the Iberian Peninsula, where the EHCs correlated well with the distribution of Solutrean point types (Schmidt, 2015a, b). The EHCs give one exploratory scenario as to why Germany and the Netherlands have so little evidence of human occupation despite the high HEP in these regions. Based on the BPP analysis, we suggest stable contact between Solutrean Core Areas in France and northern Iberia. The dispersal of Solutrean groups into southern Iberia is modeled along the coast, while the inland might have provided corridors during intermittent phases in a changing climate (see also Weniger et al., 2019).

As demonstrated with the BPP method, HEP is a valuable quantity to estimate the likeliness of contact and dispersal processes of hunter-gatherers based on climatic and environmental conditions. In agent-based (Wren and Burke, 2019) or dynamic human dispersion models (e.g., Steele, 2009; Timmermann and Friedrich, 2016), HEP can be used to define the attractiveness of a region for human existence, providing thereby a common ground between HEP-based human dispersion models and agent-based models.

Declaration of competing interest

The authors declare that they have no known competing financial interests or personal relationships that could have appeared to influence the work reported in this paper.

Acknowledgments

The authors thank Andreas Zimmermann (University of Cologne), Andreas Hense (University of Bonn) and two anonymous reviewers for their comments and discussions that helped to improve the paper. This paper was developed within the framework of the CRC 806 (project ID 57444011) and funded by the Deutsche Forschungsgemeinschaft (DFG, German Research Foundation). All simulations were performed at the German Climate Computing Center (DKRZ) within Project 965.

Appendices.

A. Bioclimatic variables

To evaluate the bioclimatic variables, monthly temperature (T) and precipitation (P), and daily maximum temperature (Tx) and minimum temperature (Tn) values on a curvilinear grid with approx. 0.5° resolution of a 30 years time series are used. The calculations are performed for each gird point separately (not shown in the equations).

A.1. Annual Mean Temperature

$$\text{Bio}\quad 1 = \frac{1}{30}\sum_{i=1}^{30}\left(\frac{1}{12}\sum_{j=1}^{12} T((i-1)\cdot 12 + j)\right) \tag{12}$$

A.2. Mean Diurnal Range

$$\text{Bio}\quad 2 = \frac{1}{10958}\sum_{i=1}^{10958}(Tx(i) - Tn(i)) \tag{13}$$

A.3. Isothermality

$$\text{Bio}\quad 3 = \text{BIO}\quad 2/\text{BIO}\quad 7\cdot 100 \tag{14}$$

A.4. Temperature Seasonality

$$\text{Bio}\quad 4=\frac{1}{30}\sum_{i=1}^{30}\sqrt{\frac{1}{12}\sum_{j=1}^{12}\left(T((i-1)\cdot 12+j)-\overline{T_i}\right)^2}, \tag{15}$$

while $\overline{T_i}$ is the mean Temperature of the year *i*.

A.5. Max Temperature of Warmest Month

Txm is the monthly mean maximum temperature. For $j \in [1,12]$:

$$\text{Bio}\quad 5=\max_j\left(\frac{1}{30}\sum_{i=1}^{30}\left(\text{Txm}\left(\left(i-1\right)\cdot 12+j\right)\right)\right) \tag{16}$$

A.6. Min Temperature of Coldest Month

Tnm is the monthly mean minimum temperature. For $j \in [1,12]$:

$$\text{Bio}\quad 6=\min_j\left(\frac{1}{30}\sum_{i=1}^{30}(\text{Tnm}((i-1)\cdot 12+j))\right) \tag{17}$$

A.7. Temperature Annual Range

$$\text{Bio}\quad 7=\text{BIO}\quad 5-\text{BIO}\quad 6 \tag{18}$$

A.8. Mean Temperature of Wettest Quarter

For each month the precipitation of two consecutive months have been added to get 12 different quarterly precipitations (*PQ*). For the quarterly precipitation of November and December the precipitation of the following year have been added. In the last year the precipitation of January respectively January and February of the same year is taken. Then, the quarterly precipitation is averaged over the 30 years.

$$PQ_k=\frac{1}{30}\sum_{i=1}^{30}\left(\sum_{j=k}^{k+2}P((i-1)\cdot 12+j)\right),\text{with}\ \ k\in[1,\ 12], \tag{19}$$

for $i = 30$ and $k = 11$ and 12 as described in the text.

The quarterly temperature (*TQ*) is calculated in the same way, but taking the average over 3 month instead of accumulating.

$$TQ_k=\frac{1}{30}\sum_{i=1}^{30}\left(\frac{1}{3}\sum_{j=k}^{k+2}T((i-1)\cdot 12+j)\right),\text{with}\ \ k\in[1,\ 12], \tag{20}$$

for $i = 30$ and $k = 11$ and 12 as described in the text.

For $k \in [1,12]$, where: $PQ_m = \max_k PQ_k$

$$\text{Bio}\quad 8=TQ_m \tag{21}$$

A.9. Mean Temperature of Driest Quarter

For $k \in [1,12]$, where: $PQ_m = \min_k PQ_k$

$$\text{Bio}\quad 9=TQ_m \tag{22}$$

A.10. Mean Temperature of Warmest Quarter

For $k \in [1,12]$, where: $TQ_m = \max_k TQ_k$

$$\text{Bio}\quad 10=TQ_m \tag{23}$$

A.11. Mean Temperature of Coldest Quarter

For $k \in [1,12]$, where: $TQ_m = \min_k TQ_k$

$$\text{Bio}\quad 11 = TQ_m \tag{24}$$

A.12. Annual Precipitation

$$\text{Bio}\quad 12 = \frac{1}{30}\sum_{i=1}^{30}\left(\sum_{j=1}^{12} P((i-1)\cdot 12 + j)\right) \tag{25}$$

A.13. Precipitation of Wettest Month

$$\text{Bio}\quad 13 = \frac{1}{30}\sum_{i=1}^{30}\max_j(P((i-1)\cdot 12 + j)), \text{with } j \in [1,\ 12], \tag{26}$$

A.14. Precipitation of Driest Month

$$\text{Bio}\quad 14 = \frac{1}{30}\sum_{i=1}^{30}\min_j(P((i-1)\cdot 12 + j)), \text{with } j \in [1,\ 12], \tag{27}$$

A.15. Precipitation Seasonality

$$\text{Bio}\quad 15 = \frac{1}{30}\sum_{i=1}^{30}\left(\frac{\sqrt{\frac{1}{12}\sum_{j=1}^{12}\left(P((i-1)\cdot 12 + j) - \overline{P_i}\right)^2}}{\overline{P_i}}\right), \tag{28}$$

while $\overline{P_i}$ is the mean precipitation of the year *i*.

A.16. Precipitation of Wettest Quarter

For $k \in [1,12]$, where: $PQ_m = \max_k PQ_k$

$$\text{Bio}\quad 16 = PQ_m \tag{29}$$

A.17. Precipitation of Driest Quarter

For $k \in [1,12]$, where: $PQ_m = \min_k PQ_k$

$$\text{Bio}\quad 17 = PQ_m \tag{30}$$

A.18. Precipitation of Warmest Quarter

For $k \in [1,12]$, where: $TQ_m = \max_k TQ_k$

$$\text{Bio}\quad 18 = PQ_m \tag{31}$$

A.19. Precipitation of Coldest Quarter

For $k \in [1,12]$, where: $TQ_m = \min_k TQ_k$

$$\text{Bio}\quad 19 = PQ_m \tag{32}$$

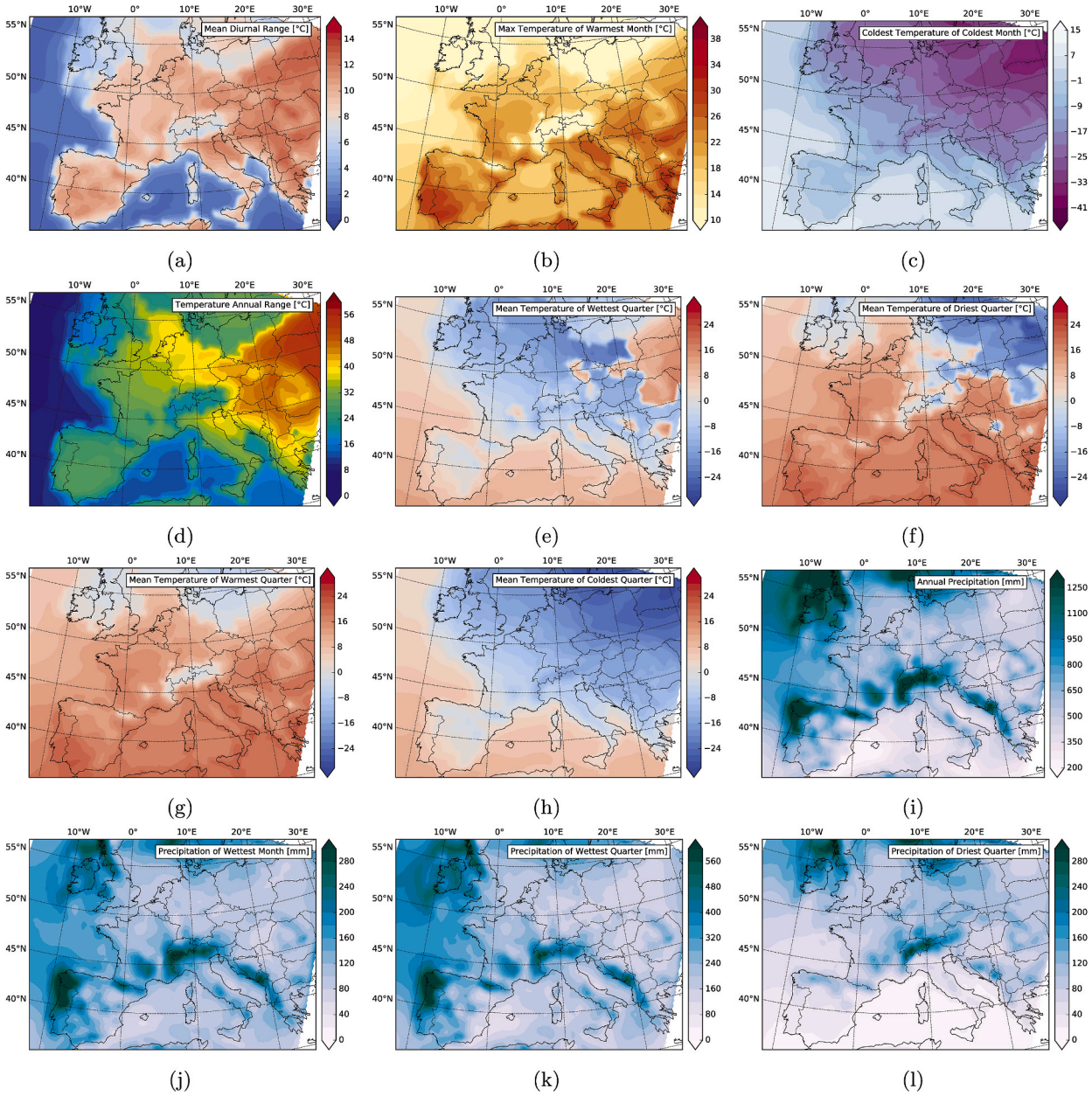

Fig. A.1. Climate maps of the bioclimatic variables not used to calculate the HEP

B. Correlation Clustering

The correlation clustering of the seven predictors remaining after VIF analysis is shown in Fig. B.1. To reduce the amount of predictors, four main branches are defined by choosing a threshold distance score of 0.3. One variable is taken from each branch.

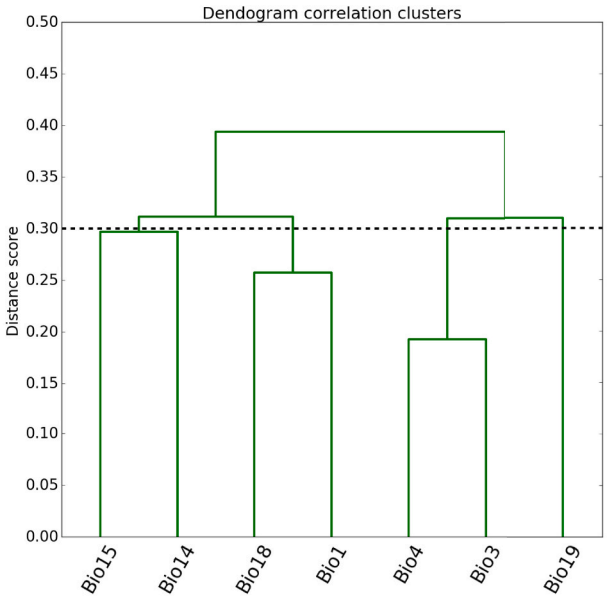

Fig. B.1. Hierarchical dendogram correlation clustering calculated from the seven bioclim variables determined after VIF analysis

C. Topography around the archaeological sites

We evaluate the average and the standard deviation of the elevation of a 30 s topographic dataset (Shao et al., 2018) by joining them to cells representing a 10 min grid. The elevation and standard deviation of elevation of each archaeological site is taken from the 10 min grid cell it is located in. Fig. C.1 shows the probability of a site to have a specific elevation level. Fig. C.2 shows the probability of a site to feature a specific elevation complexity. The lower and upper limits listed in Table 4 are chosen based on the characteristics of the histograms.

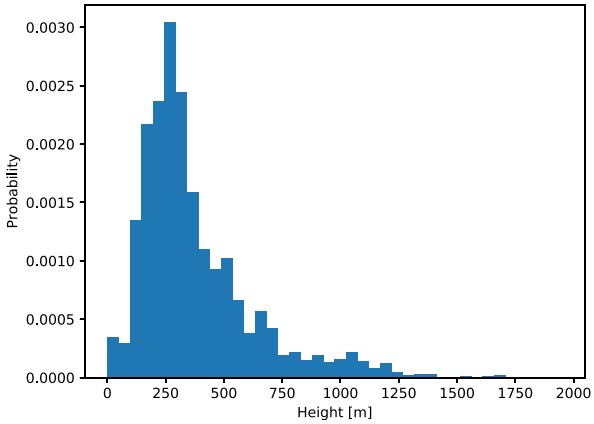

Fig. C.1. Histogram of sites with their elevation.

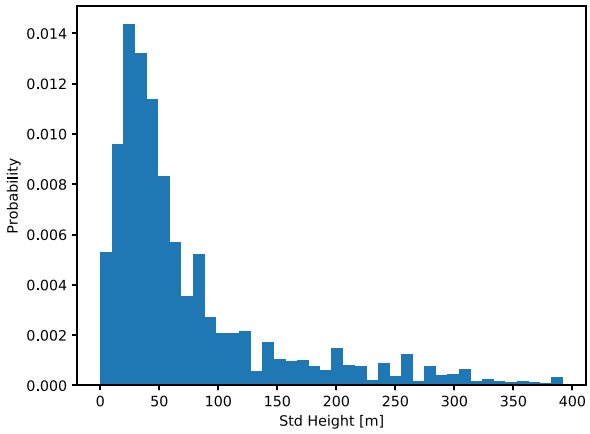

Fig. C.2. Histogram of sites with their complexity (std) of elevation.

D. Sensitivity analysis of the HEP model

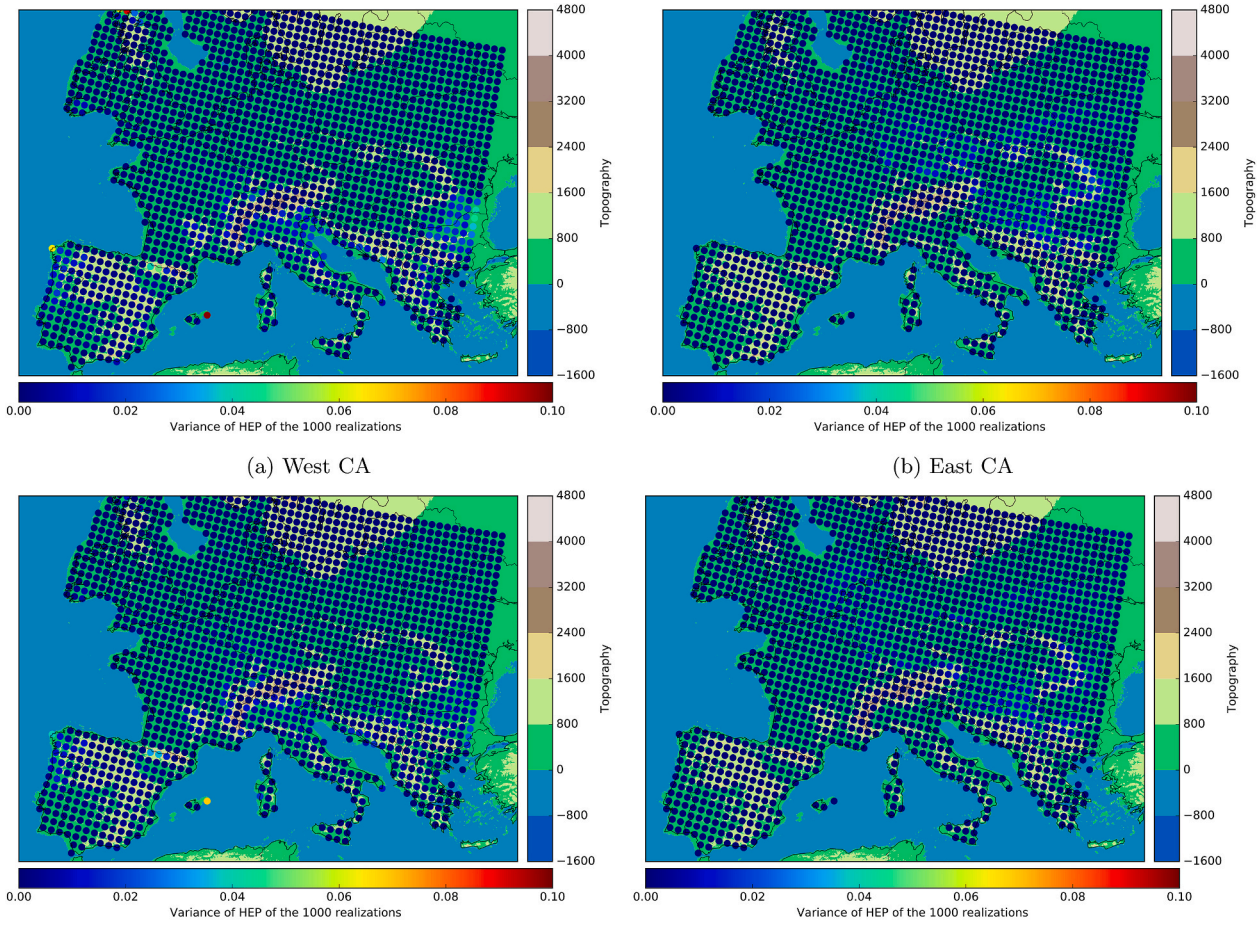

(a) West CA

(b) East CA

(c) West All

(d) East All

Fig. D.1. Local variance of HEP of the 1000 realizations per grid for a) HEP West CA, b) HEP East Ca, c) HEP West All, and d) HEP East All (depicted topography from Shao et al., 2018).

References

Alcaraz-Castaño, M., Alcolea-González, J.-J., Balbín-Behrmann, R., Kehl, M., Weniger, G.-C., 2019. Recurrent human occupations in central iberia around the last glacial maximum. The solutrean sequence of Peña Capón updated. In: Bicho, N., Cascalheira, J., Schmidt, I. (Eds.), Human Adaptations to the Last Glacial Maximum: The Solutrean and its Neighbors. Cambridge Scholar Publishing, Newcastle upon Tyne, ISBN 978-1-5275-3848-1, pp. 148–170.

Alin, A., May 2010. Multicollinearity. Wiley Interdiscip. Rev.: Comput. Stat. 2 (3), 370–374. https://doi.org/10.1002/wics.84.
Annan, J.D., Hargreaves, J.C., Feb. 2013. A new global reconstruction of temperature changes at the Last Glacial Maximum. Clim. Past 9 (1), 367–376. https://doi.org/10.5194/cp-9-367-2013.
Banks, W.E., Zilhão, J., d'Errico, F., Kageyama, M., Sima, A., Ronchitelli, A., 2009. Investigating links between ecology and bifacial tool types in western europe during the last glacial maximum. J. Archaeol. Sci. 36 (12), 2853–2867. https://doi.org/10.1016/j.jas.2009.09.014.
Banks, W.E., d'Errico, F., Zilhão, J., 2013. Human–climate interaction during the early upper paleolithic: testing the hypothesis of an adaptive shift between the proto-aurignacian and the early aurignacian. J. Hum. Evol. 64 (1), 39–55. https://doi.org/10.1016/j.jhevol.2012.10.001.
Bartlein, P.J., Harrison, S.P., Brewer, S., Connor, S., Davis, B.A.S., Gajewski, K., Guiot, J., Harrison-Prentice, T.I., Henderson, A., Peyron, O., Prentice, I.C., Scholze, M., Seppä, H., Shuman, B., Sugita, S., Thompson, R.S., Viau, A.E., Williams, J., Wu, H., Aug. 2011. Pollen-based continental climate reconstructions at 6 and 21 ka: a global synthesis. Clim. Dynam. 37 (3–4), 775–802. https://doi.org/10.1007/s00382-010-0904-1.
Becker, D., De Andrés-Herrero, M., Willmes, C., Weniger, G.-C., Bareth, G., 2017. Investigating the influence of different dems on gis-based cost distance modeling for site catchment analysis of prehistoric sites in andalusia. ISPRS Int. J. Geo-Inf. 6 (2) https://doi.org/10.3390/ijgi6020036.
Binford, L., 2002. Constructing frames of reference: an analytical method for archeological theory building using ethnographic and environmental data sets. J. Anthropol. Res. 58 (3), 416–419. https://doi.org/10.1086/jar.58.3.3631188.
Bocquet-Appel, J.-P., Demars, P.-Y., Noiret, L., Dobrowsky, D., 2005. Estimates of upper palaeolithic meta-population size in europe from archaeological data. J. Archaeol. Sci. 32 (11), 1656–1668. https://doi.org/10.1016/j.jas.2005.05.006.
Braconnot, P., Harrison, S.P., Kageyama, M., Bartlein, P.J., Masson-Delmotte, V., Abe-Ouchi, A., Otto-Bliesner, B., Zhao, Y., June 2012. Evaluation of climate models using palaeoclimatic data. Nat. Clim. Change 2 (6), 417–424. https://doi.org/10.1038/nclimate1456.
Bradtmöller, M., Pastoors, A., Weninger, B., Weniger, G.-C., Jan. 2012. The repeated replacement model – rapid climate change and population dynamics in Late Pleistocene Europe. Quat. Int. 247, 38–49. https://doi.org/10.1016/j.quaint.2010.10.015.
Burke, A., Kageyama, M., Latombe, G., Fasel, M., Vrac, M., Ramstein, G., James, P.M., 2017. Risky business: the impact of climate and climate variability on human population dynamics in Western Europe during the Last Glacial Maximum. Quat. Sci. Rev. 164, 217–229. https://doi.org/10.1016/j.quascirev.2017.04.001.
Dormann, C.F., Elith, J., Bacher, S., Buchmann, C., Carl, G., Carré, G., Marquéz, J.R.G., Gruber, B., Lafourcade, B., Leitão, P.J., Münkemüller, T., McClean, C., Osborne, P.E., Reineking, B., Schröder, B., Skidmore, A.K., Zurell, D., Lautenbach, S., Jan. 2013. Collinearity: a review of methods to deal with it and a simulation study evaluating their performance. Ecography 36 (1), 27–46. https://doi.org/10.1111/j.1600-0587.2012.07348.x.
French, J.C., Collins, C., Mar. 2015. Upper Palaeolithic population histories of Southwestern France: a comparison of the demographic signatures of 14c date distributions and archaeological site counts. J. Archaeol. Sci. 55, 122–134. https://doi.org/10.1016/j.jas.2015.01.001.
Grove, M., June 2018. Hunter-gatherers adjust mobility to maintain contact under climatic variation. J. Archaeol. Sci.: Rep. 19, 588–595. https://doi.org/10.1016/j.jasrep.2018.04.003.
Hanley, J.A., McNeil, B.J., Apr. 1982. The meaning and use of the area under a receiver operating characteristic (ROC) curve. Radiology 143 (1), 29–36. https://doi.org/10.1148/radiology.143.1.7063747.
Hijmans, R.J., Cameron, S.E., Parra, J.L., Jones, P.G., Jarvis, A., Dec. 2005. Very high resolution interpolated climate surfaces for global land areas. Int. J. Climatol. 25 (15), 1965–1978. https://doi.org/10.1002/joc.1276.
Kelly, R., 2013. The Lifeways of Hunter-Gatherers: the Foraging Spectrum. Cambridge University Press, ISBN 9781107355095.
Kondo, Y., Sano, K., Omori, T., Abe-Ouchi, A., Chan, W.-L., Kadowaki, S., Naganuma, M., O'ishi, R., Oguchi, T., Nishiaki, Y., Yoneda, M., 2018. Ecological niche and least-cost path analyses to estimate optimal migration routes of initial upper palaeolithic populations to Eurasia. In: The Middle and Upper Paleolithic Archeology of the Levant and beyond, Replacement of Neanderthals by Modern Humans Series. Springer, Singapore, pp. 199–212. https://doi.org/10.1007/978-981-10-6826-313.
Kretschmer, I., 2015. Demographische Untersuchungen zu Bevölkerungsdichten, Mobilität und Landnutzungsmustern im späten Jungpaläolithikum. Kölner Studien zur Prähistorischen Archäologie 6. VML Vlg Marie Leidorf, Rahden.
Ludwig, P., Pinto, J.G., Raible, C.C., Shao, Y., May 2017. Impacts of surface boundary conditions on regional climate model simulations of European climate during the Last Glacial maximum: regional European climate during the LGM. Geophys. Res. Lett. 44 (10), 5086–5095. https://doi.org/10.1002/2017GL073622.
Ludwig, P., Shao, Y., Kehl, M., Weniger, G.-C., 2018. The Last Glacial Maximum and Heinrich event I on the Iberian Peninsula: a regional climate modelling study for understanding human settlement patterns. Global Planet. Change 170, 34–47. https://doi.org/10.1016/j.gloplacha.2018.08.006.
Ludwig, P., Gómez-Navarro, J.J., Pinto, J.G., Raible, C.C., Wagner, S., Zorita, E., 2019. Perspectives of regional paleoclimate modeling. Ann. N. Y. Acad. Sci. 1436 (1), 54–69. https://doi.org/10.1111/nyas.13865.
Maier, A., Zimmermann, A., 2015. CRC806-E1 LGM-Sites Database V-20150313.
Maier, A., Zimmermann, A., 2017. Populations headed south? the gravettian from a palaeodemographic point of view. Antiquity 91 (357), 573–588. https://doi.org/10.15184/aqy.2017.37.
Maier, A., Lehmkuhl, F., Ludwig, P., Melles, M., Schmidt, I., Shao, Y., Zeeden, C., Zimmermann, A., 2016. Demographic estimates of hunter–gatherers during the last glacial maximum in europe against the background of palaeoenvironmental data. Quat. Int. 425, 49–61. https://doi.org/10.1016/j.quaint.2016.04.009.
Maier, A., Ludwig, P., Zimmermann, A., Schmidt, I., 2020. The sunny side of the Ice Age: solar insolation as a potential long-term pacemaker for demorgraphic developments in Europe between 43 and 15 ka ago (accepted manuscript). PaleoAnthropology.
Marami Milani, M., Hense, A., Rahmani, E., Ploeger, A., July 2016. Applying least Absolute shrinkage selection operator and akaike information criterion analysis to find the best multiple linear regression models between climate indices and components of cow's milk. Foods 5 (4), 52. https://doi.org/10.3390/foods5030052.
Müller, U.C., Pross, J., Tzedakis, P.C., Gamble, C., Kotthoff, U., Schmiedl, G., Wulf, S., Christanis, K., 2011. The role of climate in the spread of modern humans into europe. Quat. Sci. Rev. 30 (3), 273–279. https://doi.org/10.1016/j.quascirev.2010.11.016.
Müllner, D., 2013. fastcluster: fast hierarchical, agglomerative clustering routines for r and python. J. Stat. Softw. 53 (9), 1–18. https://doi.org/10.18637/jss.v053.i09.
O'Donnell, M.S., Ignizio, D.A., 2012. Bioclimatic predictors for supporting ecological applications in the conterminous United States. U.S. Geological Survey Data Series 691, 10.
Schmidt, I., 2015a. Beyond solutrean point types: technological organization and behavioral implications. J. Anthropol. Res. 71 (4), 493–508. https://doi.org/10.3998/jar.0521004.0071.402.
Schmidt, I., 2015b. Solutrean points of the iberian Peninsula. Tool making and using behaviour of hunter-gatherers during the last glacial maximum. BAR Int. Ser. 2778 https://doi.org/10.30861/9781407314709.
Schmidt, I., Bradtmöller, M., Kehl, M., Pastoors, A., Tafelmaier, Y., Weninger, B., Weniger, G.-C., 2012. Rapid climate change and variability of settlement patterns in Iberia during the Late Pleistocene. Quat. Int. 274, 179–204. https://doi.org/10.1016/j.quaint.2012.01.018.
Schmidt, I., Hilpert, J., Kretschmer, I., Peters, R., Broich, M., Schiesberg, S., Vogles, O., Wendt, K., Zimmermann, A., Maier, A., 2020. Approaching prehistoric demography: proxies, scales and scopes of the Cologne protocol for the European context. In: Proceedings of the Royal Society Series B, Page to Appear.
Shao, Y., Anhäuser, A., Ludwig, P., Schlüter, P., Williams, E., Sept. 2018. Statistical reconstruction of global vegetation for the last glacial maximum. Global Planet. Change 168, 67–77. https://doi.org/10.1016/j.gloplacha.2018.06.002.
Skamarock, W., Klemp, J., Dudhia, J., Gill, D., Barker, D., Wang, W., Huang, X.-Y., Duda, M., jun 2008. A Description of the Advanced Research WRF Version 3. Technical Report. UCAR/NCAR.
Steele, J., Apr. 2009. Human dispersals: mathematical models and the archaeological record. Hum. Biol. 81 (2–3), 121–140. https://doi.org/10.3378/027.081.0302.
Stevens, B., Giorgetta, M., Esch, M., Mauritsen, T., Crueger, T., Rast, S., Salzmann, M., Schmidt, H., Bader, J., Block, K., Brokopf, R., Fast, I., Kinne, S., Kornblueh, L., Lohmann, U., Pincus, R., Reichler, T., Roeckner, E., 2013. Atmospheric component of the mpi-m earth system model: echam6. J. Adv. Model. Earth Syst. 5 (2), 146–172. https://doi.org/10.1002/jame.20015.
Straus, L.G., 1990a. The last glacial maximum in cantabrian Spain: the solutrean. In: Soffer, O., Gamble, C. (Eds.), The World at 18.000 BP: High Latitudes. Unwin Hyman, London, pp. 88–108.
Straus, L.G., 1990b. The original arms race: Iberian perspectives on the solutrean phenomenon. In: Kozlowski, J. (Ed.), Feuilles de Pierre. Les industries à pointes folliacées du paléolithique supérieur européen. ERAUL, Liège, pp. 425–447. Actes du Colloque de Cracovie.
T, R., Hastie, T., Friedman, J., 2008. The Elements of Statistical Learning: Data Mining, Inference, and Prediction, second ed. Springer.
Tallavaara, M., Luoto, M., Korhonen, N., Järvinen, H., Seppä, H., 2015. Human population dynamics in europe over the last glacial maximum. Proc. Natl. Acad. Sci. Unit. States Am. 112 (27), 8232–8237. https://doi.org/10.1073/pnas.1503784112.
Tibshirani, R., 1996. Regression shrinkage and selection via the lasso. J. Roy. Stat. Soc. B 58 (1), 267–288. ISSN 359246.
Timmermann, A., Friedrich, T., Oct. 2016. Late Pleistocene climate drivers of early human migration. Nature 538 (7623), 92–95. https://doi.org/10.1038/nature19365.
Tzedakis, P.C., Hughen, K.A., Cacho, I., Harvati, K., 2007. Placing late neanderthals in a climatic context. Nature 449, 206–208.
van Andel, T.H., Davies, W. (Eds.), 2003. Neanderthals and Modern Humans in the European Landscape during the Last Glaciation: Archaeological Results of the Stage 3 Project. McDonald Institute for Archaeological Research monographs.
Vita-Finzi, C., Higgs, E.S., Sturdy, D., Harriss, J., Legge, A.J., Tippett, H., 1970. Prehistoric economy in the mount carmel area of Palestine: site catchment analysis. Proc. Prehist. Soc. 36 (1–37) https://doi.org/10.1017/S0079497X00013074.

Weniger, G.-C., de Andrés-Herrero, M., Bolin, V., Kehl, M., Otto, T., Potì, A., Tafelmaier, Y., 2019. Late glacial rapid climate change and human response in the westernmost mediterranean (iberia and Morocco). PLoS One 14 (12), 1–33. https://doi.org/10.1371/journal.pone.0225049, 12.

White, D., Surface-Evans, S., 2012. Least Cost Analysis of Social Landscapes: Archaeological Case Studies. University of Utah Press, ISBN 9781607811992.

Wren, C.D., Burke, A., June 2019. Habitat suitability and the genetic structure of human populations during the last glacial maximum (LGM) in western europe. PLoS One 14 (6), e0217996. https://doi.org/10.1371/journal.pone.0217996.

Zimmermann, A., Richter, J., Frank, T., Wendt, K.P., 2004. Landschaftsatchäologie ii: Überlegungen zu prinzipien einer landschaftsarchäologie. Berichte der Römisch-Germanischen Komission 85, 37–95.

Zimmermann, A., Hilpert, J., Wendt, K.P., 2009. Estimations of population density for selected periods between the neolithic and ad 1800. Hum. Biol. 81, 357–380. https://doi.org/10.3378/027.081.0313.